2016-06

Water tunnel studies of dynamic wing flap effects

Gonz‡lez, Edgar E.

Monterey, California: Naval Postgraduate School

NAVAL POSTGRADUATE SCHOOL

MONTEREY, CALIFORNIA

THESIS

WATER TUNNEL STUDIES OF DYNAMIC WING FLAP EFFECTS

by

Edgar E. González

June 2016

Thesis Advisor: M. S. Chandrasekhara
Second Reader: Kevin D. Jones

Approved for public release; distribution is unlimited

THIS PAGE INTENTIONALLY LEFT BLANK

REPORT DOCUMENTATION PAGE

Form Approved OMB No. 0704-0188

1. AGENCY USE ONLY ***(Leave blank)***	**2. REPORT DATE** June 2016	**3. REPORT TYPE AND DATES COVERED** Master's Thesis

4. TITLE AND SUBTITLE
WATER TUNNEL STUDIES OF DYNAMIC WING FLAP EFFECTS

5. FUNDING NUMBERS

6. AUTHOR(S) Edgar E. González

7. PERFORMING ORGANIZATION NAME(S) AND ADDRESS(ES)
Naval Postgraduate School
Monterey, CA 93943-5000

8. PERFORMING ORGANIZATION REPORT NUMBER

9. SPONSORING /MONITORING AGENCY NAME(S) AND ADDRESS(ES)
N/A

10.SPONSORING/MONITORING AGENCY REPORT NUMBER

11. SUPPLEMENTARY NOTES The views expressed in this thesis are those of the author and do not reflect the official policy or position of the Department of Defense or the U.S. Government. IRB Protocol number ____N/A____.

12a. DISTRIBUTION / AVAILABILITY STATEMENT
Approved for public release; distribution is unlimited

12b. DISTRIBUTION CODE

13. ABSTRACT (maximum 200 words)

The flow features developing over a two-element NACA 0012 airfoil, with the rear portion serving as a trailing edge flap, were investigated using dye flow visualization in the NPS water tunnel. The original motivation for the work arose from a need to identify any potential to enhance maneuverability of aircraft to enable smoother landing under adverse flight situations. The flap portion was maneuvered in two different unsteady motion histories by a drive mechanism: a constant pitch rate motion and a sinusoidal oscillatory motion, at Reynolds numbers of 7,500 and 37,500. Comparisons were also drawn with steady flow features under similar conditions. In both unsteady cases, features of dynamic stall flow were observed. Unlike standard airfoil dynamic stall, the unsteady flow over a dynamic flap develops in the wake of the airfoil main element. This introduces many flow complexities such as reversed flows at low flap (deflection) angles of attack, dynamic stall developing from the wrap-around trailing edge flow that also interacts with main element boundary layer flow, unusual behavior for the main element, and flap clearance gap flow. However, since dynamic stall was observed at such flap deflections, it indicates that by differentially oscillating the flaps, it might be possible to develop differential lift on the two sides of a flight vehicle, which may provide better control authority than seen in steady flows. The results could be applied to unmanned air vehicles as well.

14. SUBJECT TERMS unsteady aerodynamics, oscillatory flap, 2D-unsteady flows	**15. NUMBER OF PAGES** 73
	16. PRICE CODE

17. SECURITY CLASSIFICATION OF REPORT	**18. SECURITY CLASSIFICATION OF THIS PAGE**	**19. SECURITY CLASSIFICATION OF ABSTRACT**	**20. LIMITATION OF ABSTRACT**
Unclassified	Unclassified	Unclassified	UU

NSN 7540-01-280-5500 Standard Form 298 (Rev. 2-89)
Prescribed by ANSI Std. 239-18

THIS PAGE INTENTIONALLY LEFT BLANK

Approved for public release; distribution is unlimited

WATER TUNNEL STUDIES OF DYNAMIC WING FLAP EFFECTS

Edgar E. González
Lieutenant Commander, Mexican Navy
B.S., Mexican Naval Academy, 2002

Submitted in partial fulfillment of the
requirements for the degree of

MASTER OF SCIENCE IN MECHANICAL ENGINEERING

from the

NAVAL POSTGRADUATE SCHOOL
June 2016

Approved by: M. S. Chandrasekhara
Thesis Advisor

Kevin D. Jones
Second Reader

Garth V. Hobson
Chair, Department of Mechanical and Aerospace Engineering

THIS PAGE INTENTIONALLY LEFT BLANK

ABSTRACT

The flow features developing over a two-element NACA 0012 airfoil, with the rear portion serving as a trailing edge flap, were investigated using dye flow visualization in the NPS water tunnel. The original motivation for the work arose from a need to identify any potential to enhance maneuverability of aircraft to enable smoother landing under adverse flight situations. The flap portion was maneuvered in two different unsteady motion histories by a drive mechanism: a constant pitch rate motion and a sinusoidal oscillatory motion, at Reynolds numbers of 7,500 and 37,500. Comparisons were also drawn with steady flow features under similar conditions. In both unsteady cases, features of dynamic stall flow were observed. Unlike standard airfoil dynamic stall, the unsteady flow over a dynamic flap develops in the wake of the airfoil main element. This introduces many flow complexities such as reversed flows at low flap (deflection) angles of attack, dynamic stall developing from the wrap-around trailing edge flow that also interacts with main element boundary layer flow, unusual behavior for the main element, and flap clearance gap flow. However, since dynamic stall was observed at such flap deflections, it indicates that by differentially oscillating the flaps, it might be possible to develop differential lift on the two sides of a flight vehicle, which may provide better control authority than seen in steady flows. The results could be applied to unmanned air vehicles as well.

THIS PAGE INTENTIONALLY LEFT BLANK

TABLE OF CONTENTS

LIST OF FIGURES

LIST OF TABLES

THIS PAGE INTENTIONALLY LEFT BLANK

LIST OF ACRONYMS, ABBREVIATIONS, AND SYMBOLS

a	amplitude
α	angle of attack
α_{ME}	main element angle of attack
α_{ss}	static stall angle
$\dot{\alpha}$	pitch rate
α^+	non-dimensional pitch rate
ABS	acrylonitrile butadiene styrene
AFCA2020	Active Control for Flexible 2020 Aircraft
API	application program interface
BACT	Benchmark Active Control Technology
BWB	blended wind body
$\bar{c}$	mean chord length
c	flap chord length
CFD	Computational fluid dynamics
C_D	drag force coefficient
C_L	lift force coefficient
C_{lmax}	peak lift coefficient
C_M	pitching moment coefficient
C_N	normal force coefficient
C_r	root chord length
DDLE	dynamically deforming leading edge
f	frequency
FOF	flap oscillation frequency
k	reduced frequency
LEV	leading edge vortex
LIF	laser-induced fluorescence
M	Mach number
MAC	mean aerodynamic chord
MAE	Mechanical and Aerospace Engineering

MAV	micro-air vehicles
NACA	National Advisory Committee for Aeronautics
p	roll
q	pitch
r	yaw
Re	Reynolds number
Re_c	chord Reynolds number
ss	static stall
SST	supper sonic transport
TED	trailing-edge deflection
TEF	trailing-edge flap
UAV	unmanned aerial vehicles
U_B	average velocity in the lower surface as defined in Fig. 2
U_G	velocity as defined in Fig. 2
U_T	average velocity on the upper surface as defined in Fig. 2
U_∞	free stream fluid velocity
U.S.	United States
VDLE	variable droop leading edge
μ	viscosity
ν	kinematic viscosity
θ	Euler angle rotation about x axis
φ	Euler angle rotation about y axis
ψ	Euler angle rotation about z axis

ACKNOWLEDGMENTS

First of all, my sincerest gratitude to the Mexican Navy for giving me this wonderful opportunity, especially to Captain Alfredo R. Enriquez Delgado and Commander Mariano I. Lizarraga for the trust they invested in me and all their support during my stay at NPS.

I am grateful to Dr. M. S. Chandrasekhara for his support and patience in class, after class, and especially during the endless hours working on this research. I am deeply grateful to him for giving me the opportunity to work on this interesting project and sharing his knowledge with me. My most sincere respect for his responsibility and professionalism.

Finally, and most importantly, I would like to thank my beloved wife, Dulce Carolina, for her invaluable support day by day. Also, thanks to our beautiful daughter, Violetta Nikté, for being a motivation and inspiration in our lives.

THIS PAGE INTENTIONALLY LEFT BLANK

I. INTRODUCTION

Hard landings, loss of control and runway overruns have motivated the optimization of landing and take-off procedures. There has been interest in exploiting newly discovered and understood unsteady flow phenomena for this purpose. Dynamic stall associated with either oscillatory or ramp type pitch-up motion of a control surface offers some possibilities for taking advantage of unsteady flow. In particular, both these must be under controlled conditions to avoid the undesirable effects associated with the phenomenon. In this regard, scientists in the U.S. Navy are evaluating the usage of dynamic flaps for carrier deck landings. Some areas of their interest include evaluating the forces and moments produced by an oscillating wing flap, the effects of the resulting unsteady flow on airfoil/wing aerodynamics, and the consequences of these on the performance of the wing under critical landing conditions. Currently, there is limited knowledge available to analyze such new concepts. It is an area ripe for detailed studies ranging from computational fluid dynamics (CFD) analysis to experimental studies under different flow conditions over models that can oscillate the trailing edge flap of a two-element airfoil. It is noted here that such concepts can be extended to unmanned air vehicles which tend to be smaller and so, may be more Reynolds number sensitive. This is an area where the knowledge of the aerodynamic community is extremely limited and so, it merits detailed studies. Some related applications where dynamic flaps have been studied are in the active elevon rotor and wind turbines.

Any analytical or computational study needs to be validated against experiments. Additionally, such studies can also uncover new flow physics which can help further develop the theoretical studies by incorporating the physics so discovered. The overall problem of dynamic stall is extremely complex and differs in detail between two and three dimensional configurations due to three dimensionality effects on aspects of flow separation, compressibility, Reynolds number, turbulence effects, etc. It is recognized here that many of these cannot be easily modeled and hence, experimental data becomes an important resource to evaluate use of dynamic flaps.

This research analyzes the relevant and important details in the fluid flow produced by a NACA 0012 airfoil with a trailing edge flap configured as a two-element airfoil under simpler flow conditions to identify flow physics that may develop under dynamic flap operational conditions in the NPS water tunnel. Some of these may (those insensitive to Reynolds number such as massive flow separation effects) affect the larger scale prototypes and at higher speeds as well. Original plans included both qualitative flow visualization studies and strain gage load balance data acquisition. Due to instrumentation issues and other constraints, only flow visualization studies will be discussed. It is hoped that this qualitative analysis will shed some new insight that may help evolve the new concept into a practically useful one as well.

A. OVERVIEW

Use of trailing edge flaps for high lift and some control authority is well established in aerodynamics of landing aircraft. Most aircraft come in for landing at a small angle of incidence and the flap setting changes with flight conditions. However, when carrier landings are performed, this knowledge may have worked acceptably, but there are many other factors such as sea state, weather conditions, factors like thick dense fog, lack of visibility, night time landings etc., that demand more control authority for pilot and personnel safety. If such authority can be realized by differential dynamic flap operation to add an extra degree of roll control, for example, then a better success can be ensured. Towards this goal, oscillating a trailing edge flap seems like an attractive idea. It is well known from previous studies in unsteady aerodynamics, in particular dynamic stall [1], [2] that the peak lift coefficient, C_{lmax}, can attain values of 2.0, which is nearly twice the typical limit. However, the concomitant pitching moment variations can be destructive and so, the phenomenon has not been utilized. The details of dynamic stall occurrence, especially at low speeds will be discussed later on. Several new control schemes have been shown to be successful [3], [4] in alleviating the adverse flow behavior. Thus, the current qualitative study should only be deemed the first steps towards attaining the larger goal.

It is also noted that all published work relates to uniform approaching flow, which is far simpler than the flow over a trailing edge flap, which is in the wake of the main element and can be severely distorted depending on the flap configuration relative to the main element. Thus, a considerable amount of fundamental flow studies are needed before an evaluation of the concept can be made. Since dynamic flap motion is being considered, it is important to analyze dynamic stall flow here, which will be discussed in the next section.

B. BACKGROUND

Before proceeding further, some definitions are introduced to set the stage for proper flow discussion. The key factor is the degree of unsteadiness that when matched will produce identical flow features for model and prototype scale aircraft, under similar flow conditions (incompressible or compressible).

1. Non-dimensional Pitch Rate

When an airfoil is dynamically pitched in a ramp type motion, a non-dimensional pitch rate or also known as degree or unsteadiness, is defined as described by Equation (1), where the pitch rate ($\dot{\alpha}$) is defined in radians/sec, mean chord length ($\bar{c}$) in inches (or mm) and the freestream fluid velocity (U_∞) is in in/sec (or mm/sec).

$$\alpha^+ = \frac{\dot{\alpha}\bar{c}}{U_\infty} \tag{1}$$

2. Reduced Frequency

Similar to the non-dimensional pitch rate, the reduced frequency is also used as the parameter to define unsteadiness during situations where the airfoil is oscillated. It is as given by Equation (2).

In both cases, higher values of these quantities signify a higher degree of unsteadiness. Thus, comparing within a range of values will establish the effects of unsteadiness on the flow features.

Experiments conducted to study the unsteady aerodynamic behavior show how variations of the pressure coefficient and aerodynamic loads with the equivalent angle of attack have a strong sensitivity to the reduced frequency and mean angles of attack [5].

$$k = \frac{\pi f \bar{c}}{U_\infty} \tag{2}$$

3. Dynamic Stall

The dynamic-stall flow phenomenon occurs when an airfoil (or a lifting surface) is rapidly pitched past the static stall angle. It is a classic unsteady aerodynamic phenomenon and is characterized at low speed flows by a sequence of events that includes the upstream progression of the flow reversal that normally occurs near the trailing edge and the subsequent formation, convection and shedding of an energetic leading edge vortex (LEV) over the airfoil upper surface [1].

It has been shown by McCroskey [4] that dynamic stall begins near the leading edge of an airfoil and he describes its stages by analyzing the hysteresis loops of C_L, C_M, and C_D. He describes how before it occurs, the airfoil behaves as an unsteady linear thin airfoil according to the C_L and C_M trends. However, once the static stall angle α_{ss} is exceeded, a thin layer of reverse flow forms near the trailing edge.

This thin reversed flow fluid layer moves towards the leading edge and it is in this specific stage that the leading edge vortex forms. The LEV detaches (but is still connected to the leading edge through the shear layer) and moves downstream. The low pressure at the core of the vortex causes a dramatic lift increase. However, the movement of the low pressure over the airfoil upper surface during the convection phase also produces strong undesirable pitching moment variations. A secondary vortex may also form occasionally. Finally, the flow reattaches near the leading edge once α is reduced to notably lower values than α_{ss} [4] and progressively over the entire upper surface.

It has been shown by Chandrasekhara and Carr [2] that under incompressible flow conditions (at M as low as 0.3) and for low Reynolds numbers, this vortex arises from the bursting of leading edge laminar separation bubble. During its formation, the airfoil

experiences a sharp rise in lift coefficient past the static stall angle and also, a strong nose-down pitch moment due to the rapid downstream convection of the LEV and the associated center of pressure movement. After the stall begins, the fluid flow continues fully separated over the upper surface, resembling a bluff-body flow leading to an abrupt loss of lift [6]. When the airfoil angle of attack is decreased, flow eventually reattaches at an angle considerably smaller than the static angle and thus, depending on the amplitudes chosen for the airfoil movement, huge hysteresis loops form. The amplitude of motion is another critical parameter that can affect the entire sequence and angles at which the above mentioned events occur.

In order to take advantage of the beneficial effects one should attempt to manage the flow vorticity. Chandrasekhara et al. [3] reviewed several methods to control the dynamic stall. These methods were the Dynamically Deforming Leading Edge (DDLE) airfoil, the slatted airfoil, the airfoil with zero-mass flux synthetic jet and the Variable Droop Leading Edge (VDLE) airfoils, all of them as unsteady compressible flow control for helicopter rotor blade applications. However, these work for low, incompressible flow speeds as well.

Some others authors have discussed other methods like Gurney flaps and dynamic trailing edge flaps for dynamic stall control purposes. Gai and Palfrey [7] studied the usage of triangular serrated and solid Gurney flaps. They found a decrement of the zero lift by 4.5 deg. and 6 deg., respectively.

Additionally, Lee and Su [6] highlighted that “the dynamic trailing-edge flap (TEF) flow control concept is presumed to be more applicable considering the severe environment frequently encountered at the leading edge of a rotor blade, and thus has been considered extensively by researchers elsewhere for dynamic-stall flow control” [6, p.1]. The control of the dynamic flow-induced overshoot in the lift force and nose-down pitching moment could have an adverse effect. This negative effect could be attenuated by induced pulse deflection over the TEF [6].

4. Trailing Edge Effects

It is well known that an airfoil's trailing edge geometry significantly affects its performance due to the modification of the overall potential flow, which can even affect the airfoil effective shape (for example trailing edge reflex, use of a Gurney flap, etc.). These parameters directly affect the formation of the trailing wake, lift, drag and pitching moment behavior. Various types of trailing-edge flow separation control devices such as rippled trailing edge, vortex generators, and the Gurney flap have been studied to influence the above mentioned parameters [7].

The addition of the above described appendage can also influence the trailing edge camber which can also affect the Kutta condition and may result in an enhancing the design aerodynamic features of the main element and the resulting control authority.

In addition to passive devices discussed earlier, active flow control devices can be used to modulate upper and lower surface shear layers, enhancing the total airfoil circulation and, subsequently, the lift the airfoil generates at least in turbulent low Reynolds aerodynamics [8].

C. OBJECTIVES

The primary objective of this experiment is to study the physical aspects of the fluid flow over the flap by using dye-flow injection technique in the NPS water tunnel. The emphasis of this thesis is to document the flow features for a range of parameters defined by flow speed, main element mean angle, and mean angles of incidence, amplitudes, and frequencies of the flap in either ramp or a sinusoidal oscillating pitching motion about a spanwise axis.

To enable future load measurements, a prototype of the NACA 0012 model was designed and fabricated in two sections. The main element angle of attack (α_{ME}) can be varied independently of the flap attitude and its associated flap can also be deflected at will. The primary data expected is lift and pitching moment on the flap in the presence of the main element. For static and dynamic flap conditions, it will be as a function of the flap angle of attack as well.

The secondary objective of this experiment is to conduct the experiments for several non-dimensional conditions as parameters for several flow speeds and oscillating frequencies (expressed as reduced frequency) or pitch rates (non-dimensional) of the flap motion in the hope that the results can be used for larger scale models at different incompressible speeds.

It is hoped that when the study is fully completed, it will enable new developments and research in CFD to exploit the beneficial effects in oscillatory trailing edge flaps.

THIS PAGE INTENTIONALLY LEFT BLANK

II. LITERATURE SURVEY

There are several papers in literature today that discuss oscillating flaps. However, few discuss aerodynamic results for ramp-type motion for flaps. It is observed here that most of these pertain to other applications such as rotorcraft and wind turbine flow control. At times, a Gurney flap has been for lift enhancement. Control of transonic shock oscillations over wings and related problems have been attempted with this approach as well. However, none of them addresses the issues pertaining to the load effects of an oscillating wing flap, the effects of the resulting unsteady flow, and its consequences on the performance of the wing through modification of the unsteady lift load that can produce the desired changes for optimization of landing and take-off procedures. Hence, a general review of the available literature is presented before discussing the present work in the following chapters.

A study of aerodynamic loads on an oscillating NACA 0015 for rotorcraft shows how the hysteretic behavior of the dynamic load loops is affected by the actuation of the TEF. Figure 1 shows this hysteresis denoting with thick and thin lines pitch-up and pitch-down, respectively. In this experiment conducted by Lee and Su [6], the flap deflection was achieved by a pulse ramp motion in-phase and 180° out-of-phase relative to the airfoil main element. As a result, they showed that the characteristics of C_L and C_M hysteresis loops were drastically modified due to the vortex caused pressure changes around the airfoil. They highlighted that "the formation and detachment of the leading-edge vortex was found to remain largely unaffected by the flap deflection, regardless of the flap actuation start time. The low pressure signature of the vortex was, however, affected by the flap deflection. The later the flap actuation, the larger the change in the intensity of the leading-edge vortex" [6, p. 1,423].

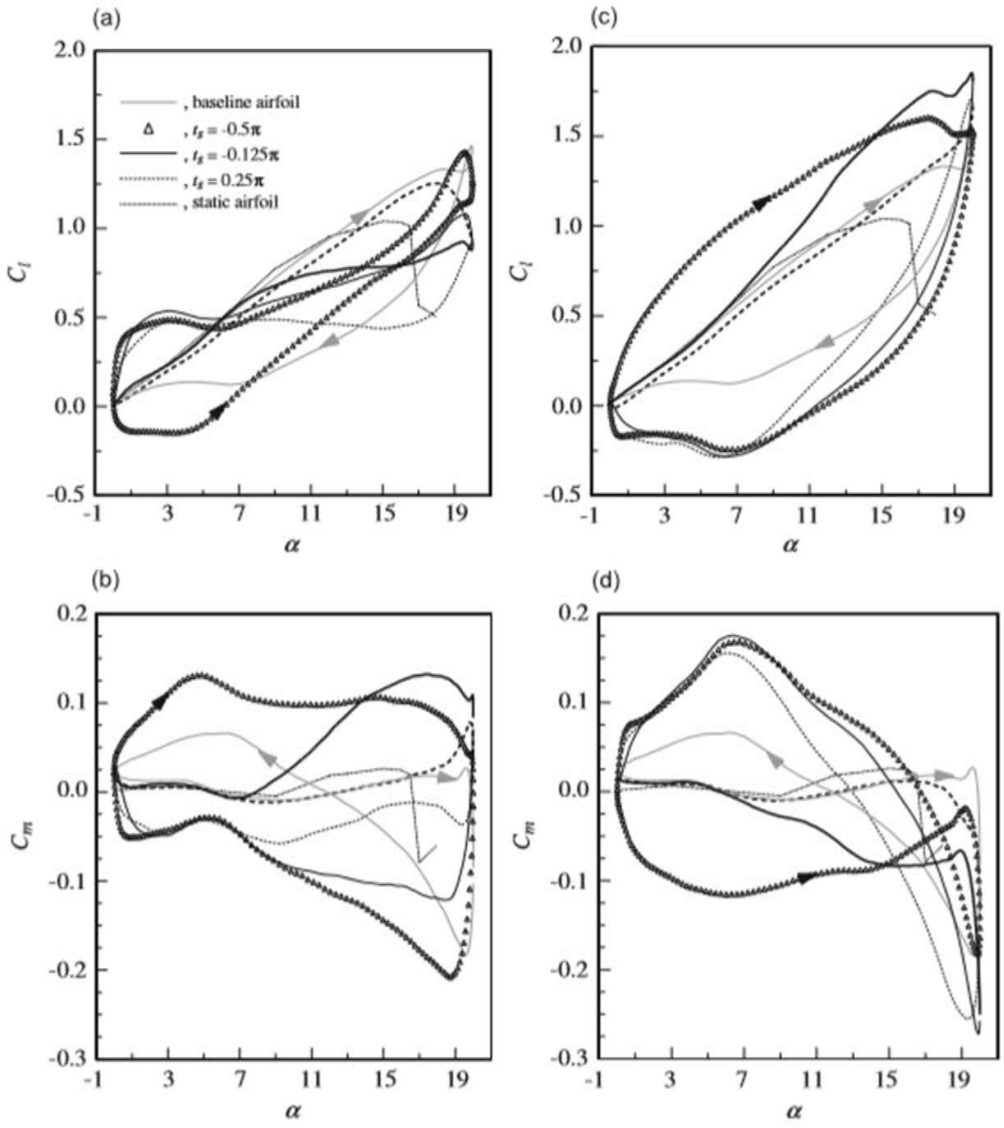

Figure 1. Dynamic load loops for (t)=10°+10°sinωt with TEF actuated at different flap actuation start time. (a)-(b) in-phase and (c)-(d) 180° out-of-phase. Source: [1].

Others have conducted experiments to study the aerodynamic flap hinge moment using the concept for control of load alleviation purposes. In this experiment, Behrens and Zhu [9] conducted a 2-D CFD study over an NACA63-200 airfoil with some modification in its TEF. Figure 2 describes the TEF with a relative thickness of 16.6% and the applied grid with a total number of grid points of 36,864.

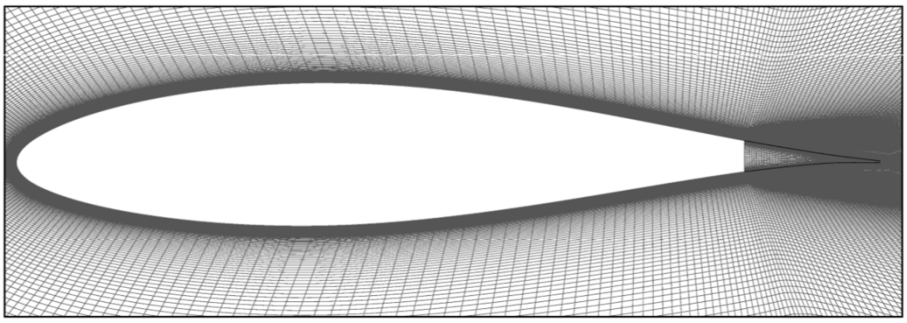

Figure 2. Close-up on the computational mesh immersed boundary. Source: [9].

Behrens and Zhu [9] applied a designed controller to the CFD simulations where the main body airfoil was defined by a conventional body and the TEF as an immersed boundary, getting successful results using the hinge moment of the trailing edge flap as sensor input. They concluded that "enhanced predictions of the hinge-moment by additional stall modeling in the potential flow model or implementing parameterized flap efficiency factors, might further improve the results" [9, p. 8].

Similarly for control purposes, the Gurney flap is another common appendage used as an effective lift enhancement method. However, it has not been used for landing or take off conditions. Due to the potentially increased camber due to flap induced flow curvature, airfoil could generate extra lift. Gai and Palfrey [7], conducted a study on a NACA 0012 airfoil with a solid and a triangular serrated Gurney flap with 5% chord length. It was innovative due to this percentage which was bigger than previously conducted studies. They have a significant result as a control method for separation flow, showing by means of oil-flow-visualization technique how the separation in the upper surface of the airfoil was practically eliminated even when the lower surface upstream in the flap presented separation (Figure 3). As a result, they found "a significant increase in $C_{l\,max}$, in the range of 65–80%, above the baseline value but a slight decrease of about 7% in the maximum lift to drag ratio" and regarding the Gurney flap, for the solid flap "the angle of zero lift decreased by six degrees and for the serrated Gurney flap decreased 4.5°" [7, p. 337]. In this context, it is noted here that Chandrasekhara [10] shows that the

optimum Gurney flap height is about 1% of the airfoil chord for the most beneficial lift enhancement effect.

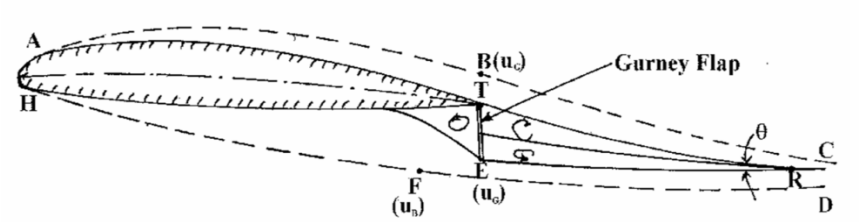

Figure 3. Flow pattern at the trailing edge with a Gurney flap. Source: [7].

Meyer and Breitsamter [11] analyzed another control method. They applied active control surfaces in a 3-D study by means of a rudder and five flaps for lateral and longitudinal control purposes, respectively. This study was addressed to analyze the steady and unsteady behavior of embedded control surfaces and describe their influence on the local and global aerodynamics. For this purpose, they selected the influence of the trailing edge flap and just one oscillating aileron (Flap5/aileron) on the blended wind body (BWB) of the Active Control for Flexible Aircraft 2020 (ACFA2020). This study was based on a limited number of test cases with time-accurate high-fidelity Euler simulation [11].

To study the influence of oscillating control surfaces on the ACFA2020 BWB aircraft, Meyer and Breitsamter [11] included the interaction of the Flap5/aileron and trailing edge flap (TEF) as shown in Figure 4. For both control surfaces, a maximum deflection angle of about two degrees was tested on steady and unsteady conditions. They concluded that increasing the oscillation frequency of the Flap5/aileron at cruise condition produced a shock on the outboard wing and consequently, this shock became unsteady whereas for the oscillatory behavior on the trailing edge deflection (TED) did not show any substantial effect [11].

Their conclusion was that “at a lower flight speed, the changes in reduced frequency are less significant. With increasing oscillation frequency, an existent recompression zone is stretched in the streamwise direction and becomes unsteady. For

both flight speeds, the oscillatory behavior of the Flap5/aileron at increasing frequency reduced the steady part of the unsteady forces and increased the unsteady part" [11, p. 633].

Meyer and Breitsamter [11] concluded that the usage of an oscillating aileron/Flap5 produced an active structural control. However, the results presented are of limited value for the general user. This is due to this control method was completely addressed to study an innovation of active control, especially of the ACFA2020 project.

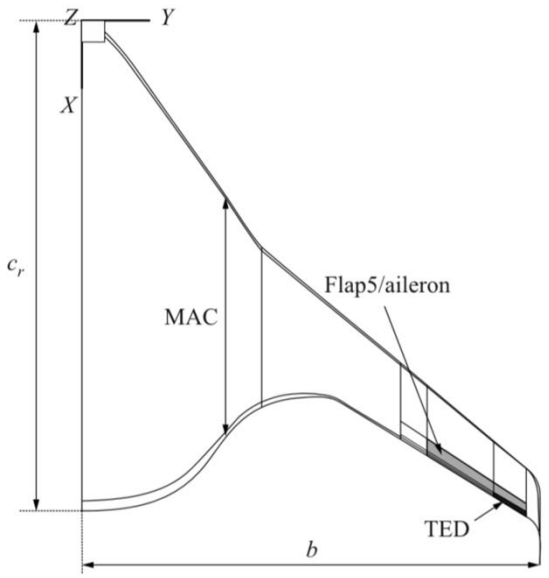

Figure 4. ACFA2020 with Flap5/aileron and TED. Source: [11].

Rampurawala and Badcock [12] investigated the aero-elastic effects (buzz) associated with control surfaces in a CFD simulation using a specific treatment which blended the flap edge into the wing. They reported how local effects of the aileron reversal impacted an F-18 wing at high speeds and also some means to control it using oscillating control surfaces. Moreover, they described instabilities such as transonic shock oscillations over wings affecting the control surfaces, particularly on trailing edges.

Their research considered a forced flap motion on a flexible wing where the flap blended into the wing using block structural grids in order to avoid surface topology changes and was able to maintain the accuracy of one-to-one grid point connectivity [12].

Their investigation was conducted on two configurations while varying the incidence, mean flap angle, Mach number, flap oscillation frequency (FOF), and flap amplitude for several cases [12]. The first configuration involved a rigid Benchmark Active Control Technology (BACT) wing model using a rectangular wing with a NACA 0012 profile in order to avoid structural deformations during the oscillatory motion in the flap. Figure 5 shows the schematic BACT model with an upper and lower surface spoiler and trailing-edge control surface [12].

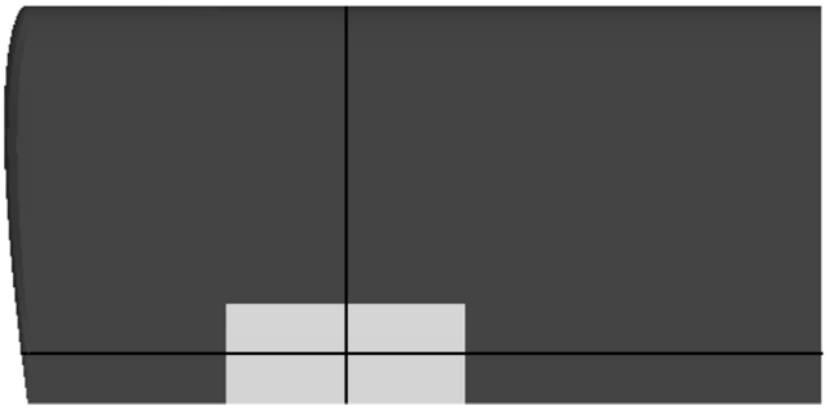

Figure 5. BACT model detail around the flap-slices used. Source: [12].

Table 1 contains the experimental details of BACT's computations. Each case shows how the model was subjected to different test conditions. In the first two cases, the model included static flap deflections of 0 and 5 degrees. In contrast, the third case was a dynamic experiment with no incidence and no mean flap deflection and with a very small flap amplitude. Simulations were run for each case in order to obtain the steady and unsteady surface pressures.

Table 1. Experimental details of the BACT case computations. Source: [12].

	Incidence	Mean flap angle	Mach no.	FOF, Hz	Flap amplitude
Case 1	−4.02 deg	0 deg	0.769	0	0 deg
Case 2	0.03 deg	5.0 deg	0.769	0	0 deg
Case 3	0 deg	0 deg	0.766	5	2.02 deg

Rampurawala and Badcock's [12] second configuration was based on supersonic transport (SST), measuring the unsteady pressure distribution over the wing, the dynamic deformation, and unsteady force coefficients. Table 2 describes the cases where flexibility in the model was considered for different flap oscillation frequencies.

Table 2. Conditions of the SST case computations. Source: [12].

	Incidence	Mean flap angle	Mach no.	FOF, Hz	Flap amplitude
Case 1	0.0 deg	0.0 deg	0.8002	10	1.203 deg
				15	1.312 deg
				20	1.116 deg
				25	1.004 deg
Case 2	−2.0 deg	0.0 deg	0.8009	10	1.567 deg
				15	1.448 deg
				20	1.229 deg
				25	1.091 deg
Case 3	−4.0 deg	5.0 deg	0.9007	5	1.844 deg
				10	1.756 deg
				20	1.284 deg

As a first approach to analyze a general dynamic behavior of the airfoil and, more specifically, the flow around the flap, both configurations were simulated. The set of data, steady and unsteady surface pressures were obtained from the BACT configuration and subsequently compared with those from the SST configuration. After the comparison of this unsteady viscous and inviscid forced flap oscillation data, they concluded that the behavior around the flap and the performance on the wing between a blended flap treatment and one simulated with gaps did not have a significant difference [12].

Finally, regarding the data obtained by means of simulations of blended edges or free edges under the BACTs cases, the results indicated that steady and unsteady cases were similar, although a small over-prediction for the maximum value of unsteadiness in the upstream direction appeared with oscillation flap motion. However, after taking into account the details of the flap edges, they found differences in the unsteady pressure coefficient magnitudes emphasizing that “the grid with the gap shows a lower level of unsteadiness with again a spike around the flap edge, suggesting that the flow through the gap provides some alleviation of the pressure changes due to the flap motion” [12, p. 1186].

Delnero [8] used a similar concept to modify the near wake of an airfoil studying aspects of the influence of an oscillating mini-flap upon the near wake of an NACA 4412 airfoil subjected to a turbulent flow field. According to the airfoil chord and the mean free stream velocity, the Reynolds number was 326,000 and 489,000. The test configuration established the turbulence intensity in 1.8%. Their study was conducted in a wind tunnel between two panels thus assuring a close approximation to a two-dimensional flow. Figure 6 is a front view of the wing model where the mini-flap located at $0.08\bar{c}$ from the trailing edge was able to oscillate around its hinge line. They varied the oscillating frequency [8].

Delnero [8] described the near-field wake characteristics as a function of flap oscillation frequency. This was done by analyzing the pressure values near the trailing edge highlighting that “the oscillating mini-flap changes the wake flow pattern, alleviating the near wake turbulence and enhancing the vortex pair near the trailing edge at the mini-flap level and below that level, magnifying the effect described first by Liebeck ” [8, p. 9].

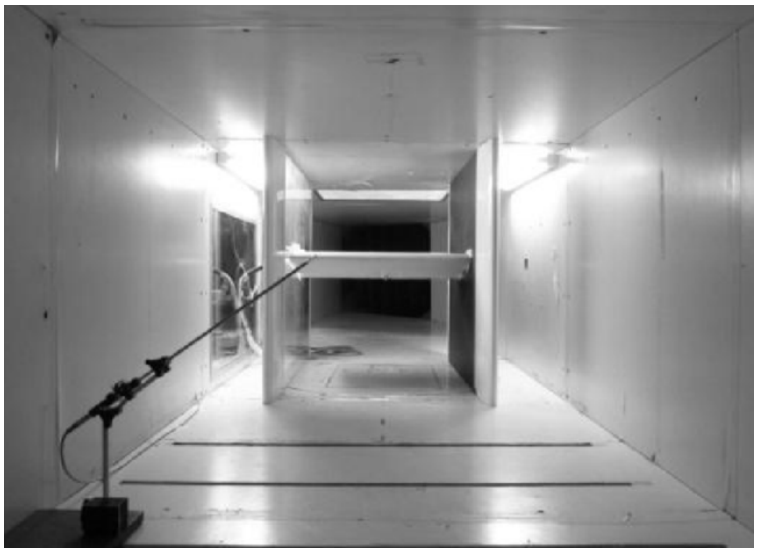

Figure 6. NACA 2212 at wind tunnel section. Source: [8].

The above brief review confirms that the results of several studies are of limited value to the specific research being planned for this thesis and do not present any coherent data or information regarding the purpose of lift enhancement (or management for roll control) under landing or take off conditions.

The importance of studying aerodynamic effects at low Reynolds numbers emerges due to a large number of applications wherein a dynamic flap can be used. Many small unmanned aerial vehicles (UAV's) and airplanes experience turbulence with length scales comparable to their span under windy conditions during landings and take-off procedures [8]. Using dynamic flaps may enable some control authority for these flight conditions.

Laitone [13] studied the lift and drag measurements on an NACA 0012 airfoil profile comparing those for thin, flat, and cambered plates at Reynolds numbers below 70,000 in a wind tunnel. He highlighted that "The lift force measurements on the NACA 0012 indicate that its sensitivity to variations of the Reynolds number or the turbulence level, make it unsuitable for all Re<50000" [13, p. 4]. Moreover, studies today of the fluid forces on airfoils at very low Reynolds numbers are becoming increasingly important due to its multiple applications and recent developments in micro-air vehicles (MAVs) and even on the smaller unmanned aerial vehicles (UAVs) [14]. As Zhou

highlighted, “General researchers on airfoil aerodynamics have focused on conventional aircraft design with Re_c beyond $5x10^5$ and α below stall” [14, p. 1].

Zhou [14] conducted a study measuring the mean and fluctuating lift and drag forces on a NACA 0012 airfoil. He analyzed the flow phenomenon using a laser-induced fluorescence (LIF) flow visualization system for α=0-90°and Re_c =5.3 x 10^3-5.1 x 10^4 [14]. He concluded that “At small Re_c, i.e. 5.3 x 10^3, there is no rapid drop in C_L nor a jump in C_D, suggesting the absence of the stall that is associated with an airfoil wake of $Re_c \geq$1.0 x 10^4,” “C_D and C_L display a strong dependence on α, as expected,” subsequently “a linear theoretical analysis is developed to predict the dependence of C_D and C_L on α” and finally “the Re_c effect on C_D and C_L depends on α” [14, p. 338].

Issac et al. [15] conducted a force measurement experiment in a water tunnel at a low Reynolds number ($\mathrm{Re}_c = 5402$ to $\mathrm{Re}_c 7054$). In this case, this study addressed micro air vehicle development applications. A flat plate wing of semi-elliptical cambered planform was submitted to a flapping-and-pitching behavior. This experiment best represents an example of the particular challenges for these kinds of conditions. Low freestream velocities, small model dimensions and a cycling motion create the perfect conditions for a difficult measurement of low force levels. Moreover, a good selection, design and location of transducer, is also convenient. Due to the fact that this type of experiment is based on cycling motion, chord Reynolds number and reduced frequency are both very important non-dimensional parameters to be used in the analysis of its performance [15].

In this section, it was realized how the influence of the aerodynamics in the main element and the resulting control authority could be integrated with phenomena akin to dynamic stall and oscillatory behaviors. This hypothesis is the motivation to improve the behavior of the platform in order to reduce the negative effects such as strong pitching moments which can affect the control as well as the generation of additional lift during landing and take-off operations.

III. DESCRIPTION OF THE PRESENT STUDIES

The studies were conducted in the Naval Postgraduate School (NPS) Mechanical and Aerospace Engineering (MAE) water tunnel on an NACA 0012 airfoil, built in two parts with a main element and a trailing edge flap. Primarily, flow visualization using colored dyes was used; however, the model used has been designed for accommodating a 5-component strain gage balance also. A range of flow conditions and flap motion histories, such as steady state, ramp and hold and, a sinusoidal oscillation, were used to qualify the effects of a dynamic flap on the flow behavior. This chapter is devoted to describing the appropriate model design details, facility used and techniques applied for flow visualization.

A. THE NPS WATER TUNNEL

The NPS water tunnel is a Model 1520 closed circuit, open channel water tunnel supplied by Rolling Hills Research Corporation (RHRC). It has been used over the years in studies of flow physics and load measurements over a variety of models and for wide ranging applications (Figure 7). Even quantitative flow visualization has been performed in it. Using a submersible 5-component strain-gage balance allows measurements of normal and side forces and the three moments, axial force cannot be measured [16].

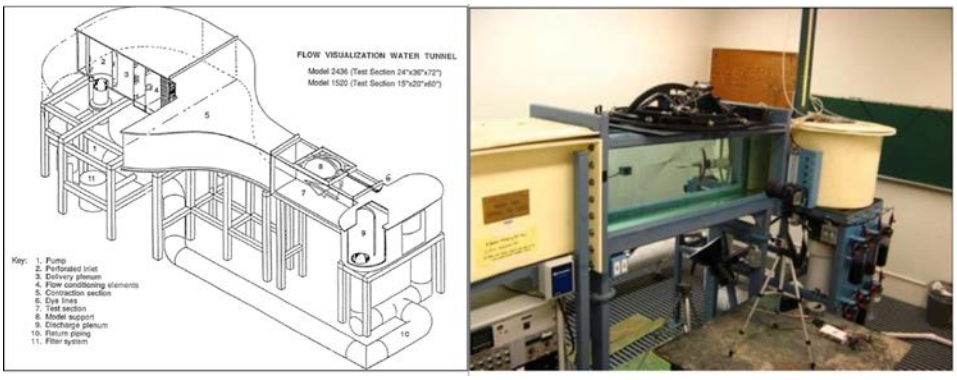

Figure 7. Naval Postgraduate School 15 in x 20 in water tunnel. Sources: [16], [17].

The test section is 15 inches wide, 20 inches deep, and 60 inches long and confined by tempered glass. The top of the channel is open and the water driven by a pump flows continuously with a free surface. The flow velocity can be continuously varied (and is software controlled) from 0 up to 1.25 ft. /sec. A rear mounted sting is used to place the model in the flow stream. The sting is connected to a C-strut, which can be moved in the pitch, roll and yaw axes (see later for more details). Additionally, the motion of the model and sting can be controlled by vendor supplied software to produce a variety of motions, which include steady, ramp-and-hold and oscillatory variation of the angle of attack over a range of angles from 0 to 40 degrees. Additionally, custom maneuvers can be executed by a computer-controlled dynamic model support system which is a hallmark of the tunnel.

B. MODEL DESIGN DETAILS

In an effort to simulate the standard wing/flap combination, a 7.38-inch total chord NACA 0012 was designed to be fabricated using rapid prototyping techniques. The flap was designed to be 1.5 in chord, making the main element chord 5.9 in The model span was set to 14.7 in, which ensured near flow two-dimensionality due to an aspect ratio of about 2. The design of the airfoil-flap combination ensured that the pitch axis coincided with its hinge line in order to effect pure flap pitch-up motion. As a consequence, the flap deflection could be specifically varied for any particular maneuver (ramp and hold, sinusoidal, etc.) of interest. Basically, the flap was attached to the sting. If the attachment included the internal balance of the water tunnel, then flap loads could be directly measured. Separate arrangements were included in the design to support the main element and vary its angle of attack. These details will be discussed in the next few sections.

1. Airfoil Model

The model was built from a NACA 0012 profile. The data file contained 120 x-y coordinates and was used to design the model according to the specification defined in Table 3.

Table 3. NACA 0012 airfoil profile model dimensions.

	Relationship with the main chord	Caption Placement
Profile		NACA 0012
Airfoil chord (with flap)	100 %	7.38 in
Flap length	20 %	1.48 in
Distance of airfoil axis of rotation from airfoil leading edge	35 %	2.58 in
Distance of flap hinge from the airfoil leading edge	80 %	5.9 in
Radius of flap leading edge		0.2 in
Gap between flap and airfoil		0.08 in
Model span		14.75 in

The model used for this investigation was constructed in acrylonitrile butadiene styrene (ABS) due to its characteristics of 3-d printer application, machinability and very smooth surface finish. It was constructed in four sections in order to avoid bending and deformation along the spanwise axis during printing.

Figure 8 shows all sections of the model. The main body airfoil was glued after embedding two dye visualization tubes for color dye injection located at $0.68\bar{c}$. Two sets of flaps were designed for this study; the first accommodated the five-component internal strain gage balance for static and dynamic load measurements while the second pair was glued after embedding three dye ports for flow visualization study. These ports were located at the leading edge of the flap (in the hinge gap), and one on the upper surface and another on the lower surface, both at approximately 90% of the flap chord. Due to the very small flap thickness, the dye ports were also small, 0.05 in diameter size.

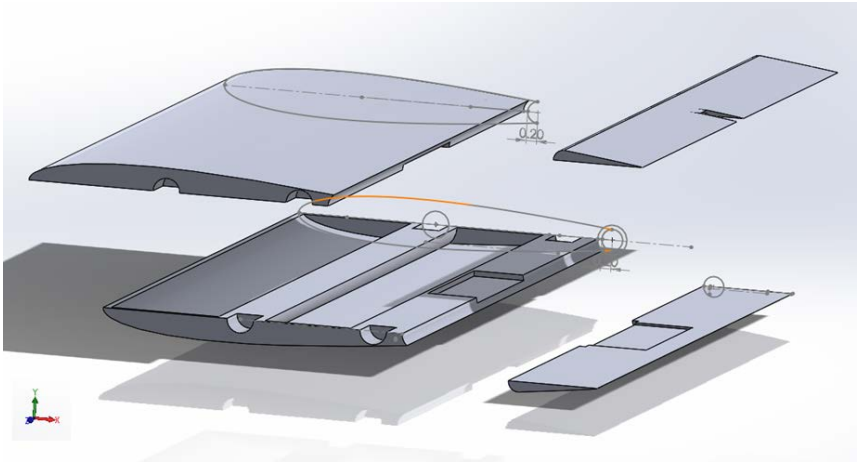

Figure 8. NACA 0012 airfoil profile model in ABS material.

2. Dynamic Model Support

The dynamic model support is shaped by a large circular anodized aluminum sector for yaw (r), (referred to as the C-strut) mounted on the yaw table aligned with the model rotation center in the vertical plane for pitch (q) and a roll motor contained in a waterproof housing. The roll motor is attached to the end of the C-strut for effecting roll motion (p). Figure 9 shows a schematic of the arrangement used.

The dynamic model support system is controlled by a National Instruments Flex Motion system with a servo motor power supply and amplifiers. A software package for experiment control, data acquisition, and data processing using National Instruments LabVIEW API with a graphical interface provides integration between the dynamic model support system, the 5-component submersible balance, and the water tunnel controls [16].

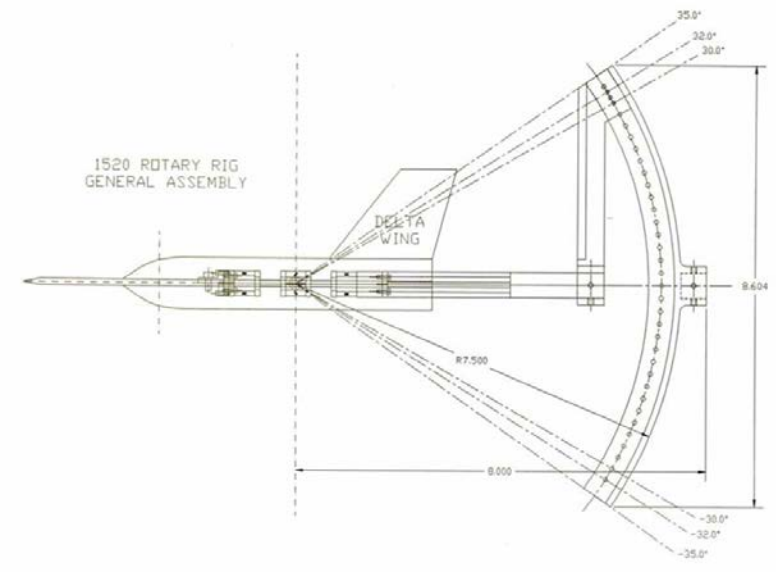

Figure 9. RHRC water tunnel rotary rig components. Source: [18].

Although multi-axis motion is possible, since the present study was concerned with the effects related to the pitching movement of the flap, only y-axis was used and x and z axes for roll and yaw channels were disconnected.

3. Airfoil Holder

As stated earlier, the main element of the airfoil/flap combination was separate from the flap itself. In an effort to provide independent variations of its parameters (angle of attack, position relative to flap, etc.) it was also supported separately from the flap. The airfoil holder was designed and built from aluminum sheet of ¼ in and 1/8 in thickness. Figure 10 shows the schematic view where 2 large strips of ¼ thicknesses were placed horizontally between the flat plates that support the C-Strut and the flat plate that contained the large circular anodized aluminum sector for yaw motion. In order to ensure the correct location of the model and maintain the arrangement fixed, this size was the maximum thickness allowed. This kept the model properly aligned with the center line of the water tunnel during the entire test process. Two sets of thin parallel strips (1/8 in thickness) were placed at $0.35\overline{c}$ and $0.68\bar{c}$, one at the center of rotation at 2.58 in from the leading edge of the airfoil and other at 5.08 in to support the alignment and keep the main element fixed during all the conditions of the entire test.

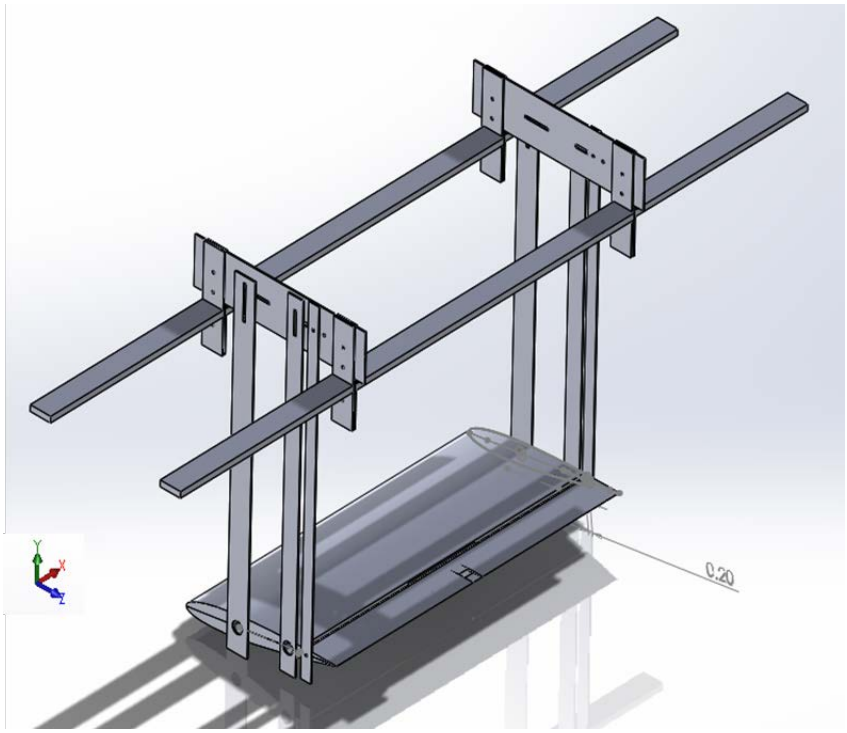

Figure 10. Aluminum airfoil holder array.

These strips held the model by a set of four stainless steels' pins of ¼ in of diameter and ½ in deep. To guaranty its free movement in 2 degrees of freedom (x- and y- axes), all of them have 1/8 in vertical slots that move over 1/8 in horizontal slots on the two vertical side plates where they are fixed by four machine screws. This configuration enabled to set the model at a wide variety of angles of attack (α). For this particular model, α was varied from 0° to 4° but, the current design permits a larger movement of $\alpha = \pm 10°$.

A third set of supplementary strips was fabricated to ensure good alignment of the flap with the main body airfoil. These were located at the center of rotation of the flap allowing a 0.08 in gap (2 mm) between the main airfoil and the flap. Its use was optional, but ensured that the two elements would not make physical contact during dynamic tests, in order to prevent mechanical damage. These struts were not used during the current experiment since it involved only flow visualization.

C. FLOW VISUALIZATION TECHNIQUE

For this particular phase of the study, the 7.5-inch long sting balance for the load measurements was not utilized. A modified shorter stainless steel sting of six inches was machined to align the center of rotation of the flap with the C-Strut's geometric center.

Five food coloring dye-injected ports were utilized to conduct flow visualization (Figure 11). Two ports were attached to the main body airfoil and three for the flap. In order to avoid the effect of buoyancy forces in the injected mixture, the food coloring was diluted to a ratio of 1:4. Because the experiment was conducted for several freestream velocities, the dye injection system was pressurized to 20 psi, and then the flow was regulated using a set of independent valves.

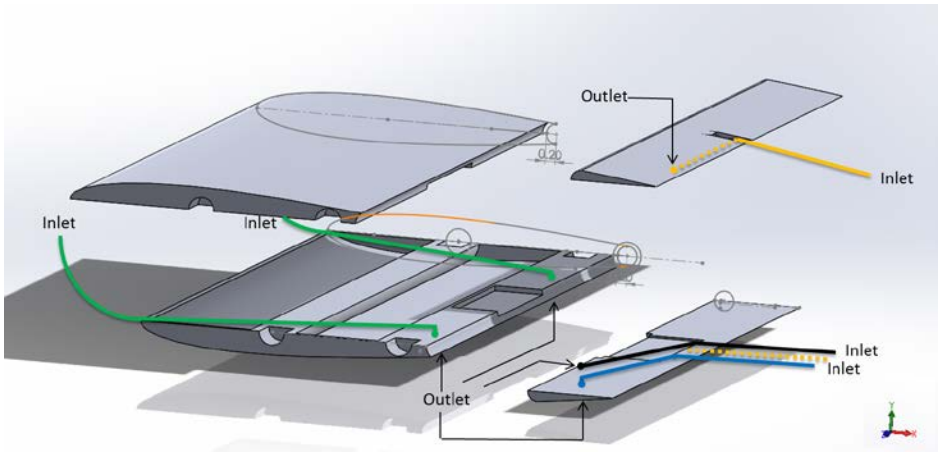

Figure 11. Five dye-injected ports.

A Nikon-D-80 camera was used to document the visualization pictures. Images were recorded from a direction orthogonal to the flap rotation in an effort to visualize the flow normal to the airfoil and on the surface itself. The shutter speed was programed at 1/200 s with an aperture setting of f/5.6 to obtain the best image quality. The camera could be externally triggered to capture pictures phase locked with the model motion as described below.

Figure 12 shows the schematic arrangement used by Chua et al. [17]. This schematic was used to obtain the image at instantaneous flap deflection (δ) when the Nikon D-80 camera was triggered remotely by a shutter control MC-DC1 which was

connected by the wire array shown in Figure 13. This system has the capability to trigger two cameras remotely. However, for the specific purposes of this study, only one camera side view was used.

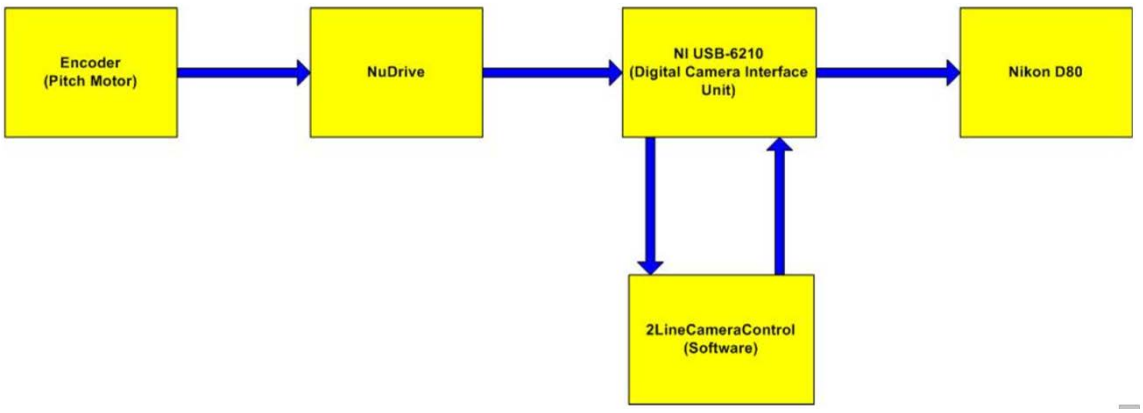

Figure 12. Schematic of phase-locked data acquisition. Source: [17].

Figure 13. Modified Nikon MC-DC1 hooked-up to Ni USB-6210 digital converter.

The Nikon D-80 camera NuDriveencoder inputs are monitored by the NIUSB-6210 digital counter input port and resolved into degrees by the software. Once the software processes the input signals from NuDrive, this addresses the trigger's signal at

the pre-defined flap deflection. The motion-control software (Figure 14) considers the number of degrees between shutter operations, fine-tunes the number of "ticks" of the encoder to optimize synchronization of degrees read, and then arms / disarms the shutters [17].

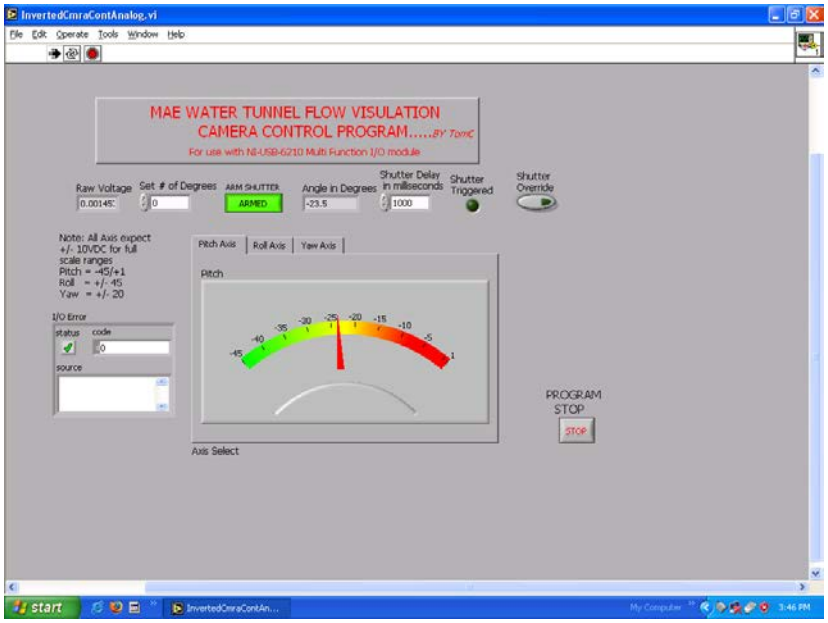

Figure 14. Motion-control software, for the Nikon D-80.

D. EXPERIMENTAL CONDITIONS

1. Flow Conditions

Based on the main chord length, the freestream flow condition was defined by its chord Reynolds number (Re_c), via Equation (6).

$$Re_c = \frac{\rho c U_\infty}{\mu} = \frac{c U_\infty}{\nu} \tag{6}$$

This calculation considered the kinematic viscosity of the water (ν) equal to 1.267E-06 m^2/s, which is shown in Table 4.

Table 4. Chord Reynolds number for experimental conditions

Fluid freestream [in/s]	$\boldsymbol{Re_c}$
2	7,500
10	37,500

2. Steady Flow

For experiments in steady flow conditions, the standard water tunnel test procedures were followed. The main body was fixed at the desired α and defined roll and yaw for the flap at zero (p=0, q=0, r=0).

To minimize the effects of the free surface, all models are mounted in the inverted position in the tunnel. Because of this, the water tunnel's C-strut geometry was preprogrammed with initial position x-y-z (θ=0°, φ=180°, ψ=0°). As a result, negative pitch (-p) movements were induced in the attached model (flap) and finally redefined as entirely negative deflection in the flap (-δ).

The tunnel speed time was programed with a settling time of 300 seconds before the static measurements were performed in order to ensure the desired free stream flow velocity was achieved. Finally, the static flow visualization was taken during a 40 seconds time period for each predefined condition.

3. Ramp and Hold Motion

This experiment was taken as the first dynamic test by varying the amplitude of the ramp. Figure 15 describes the motion history for the ramp and hold motion. In all curves, the pitch rate motion was established as $\dot{\alpha} = 1\ deg/sec$.

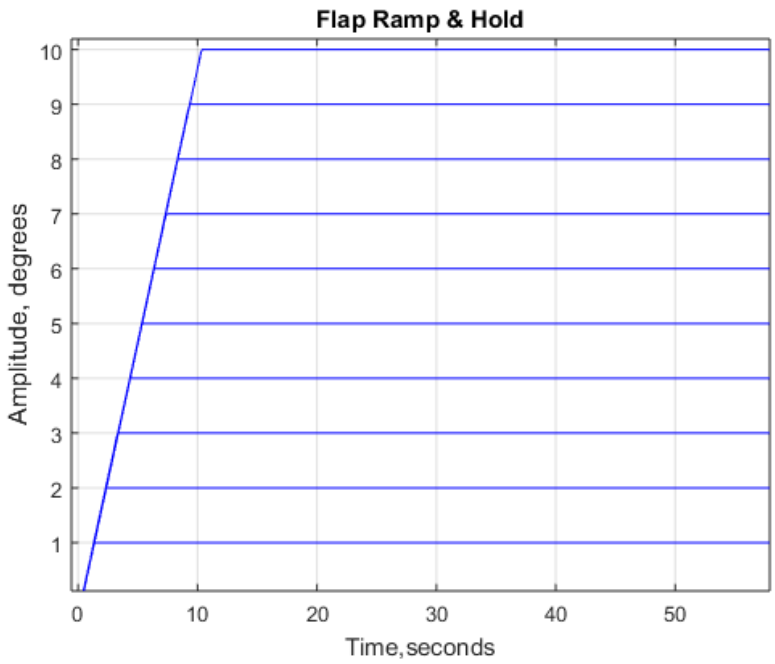

Figure 15. Motion History of the NACA 0012 model for flap for ramp and hold.

4. Oscillation

For this dynamic test, the software was programmed to generate continuous sets of ramp motions at desired amplitudes. Figure 16 describes the time history for these conditions. The flap has been moved from the initial point (0°) to the higher degree defined by the preprogramed amplitude. It can be seen how the lines show a continue slope during the positive segment and a cosine curve during the negative segment.

Each experiment was repeated 20 times for each amplitude. Regarding the flow visualization technique, it was documented during one entire cycle around the 10th to 15th repetition.

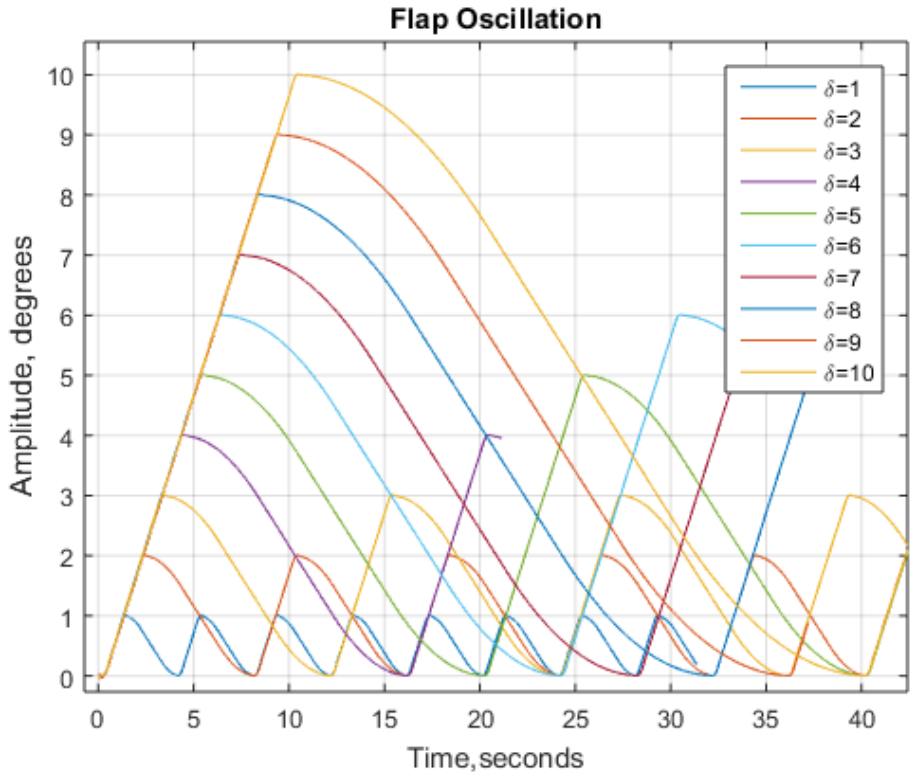

Figure 16. Motion History of the NACA 0012 model for flap oscillation.

5. Matrix or Experimental Conditions

The experiments were conducted under the described conditions in Table 5. The non-dimensional pitch rate (α^+) was also computed in order to know the degree or unsteadiness of the flap motion. Using the Equation (1) and supplying the main chord length airfoil ($\bar{c}$) by the chord length flap (c), this was defined in terms of the flap dimensions in Equation (7).

$$\alpha^+ = \frac{\dot{\alpha} c}{U_\infty} \tag{7}$$

Table 5. Chord Reynolds number for experimental conditions.

Fluid free stream (U_∞)	**2 [in/sec]**	**10 [in/sec]**
Re_c	7,500	37,500
α	0° to 4°	0° to 4°
δ	0° to 10°	0° to 10°
$\Delta\delta$	1°	1°
A	0° to 10°	0° to 10°
α^+	0.0129	0.0025
k	0.06	0.002

E. UNCERTAINTY ESTIMATION

The experimental uncertainties were considered according to previous experiments by McLain et al. [19] and Sosebee et al. [20] and were estimated in the usual manner including the uncertainties in each major component which are listed in Table 6.

Table 6. Table of measurements uncertainty.

Parameter or coefficient	**% Uncertainty**
U_∞	$\pm 4\%$
ρ	$\pm 0.2\%$

This experiment was devoted to dealing with dynamic behavior in the flap. Moreover, the angle of attack, angular deflection and pitch rate were considered to calculate experimental uncertainties related to strain gage load balance studies. This is going to be useful in establishing the actual lift forces under these flow conditions in further studies on this field.

Table 7. Table of experimental uncertainties. Source: [20].

Parameter or coefficient	**% Uncertainty**
$Normal\ Force$	$\pm 2\%$
$Moments$	$\pm 1\%$
C_N	$\pm 5\%$
C_M	$\pm 3\%$

IV. RESULTS AND DISCUSSION

In this section, key results obtained from dye-flow visualization will be presented. A discussion of steady flow features is first offered to set the stage for comparison with unsteady flow aspects as the flap is moved in specific maneuvers. It is reiterated here that to minimize free surface effects, the model was mounted in an inverted position, which should be kept in mind as the results are reviewed. In the flap only three dye ports were presented. However, only those towards the trailing edge have been used in the pictures shown. These are the red and blue dyes emanating from the lower and upper surfaces of the flap. The dye port at the flap leading edge was not used due to some interference that was noticed in the early studies. The green dye seen in the figures issues out of the upper surface of the main element.

As was mentioned before, the wing has been inverted in the tunnel. Due to this fact and in order to be consistent during the discussion, the results have been analyzed using upper/lower surface definitions as a conventional wing. Additionally, this has been done consistent with Figure 17. As a result, all the pictures taken during the study were flipped upside down to display them as right-side-up wing.

A. STEADY FLOW

Theoretically, in a wing/flap combination, with a very small gap between the two units, it is expected that the flow coming from the lower surface that has higher pressure goes through the gap and then over the upper suction surface, towards the trailing edge. Depending on the flow conditions, it may reverse and return to the lower surface as reverse flow. Figure 17 shows a schematic view of this flow pattern.

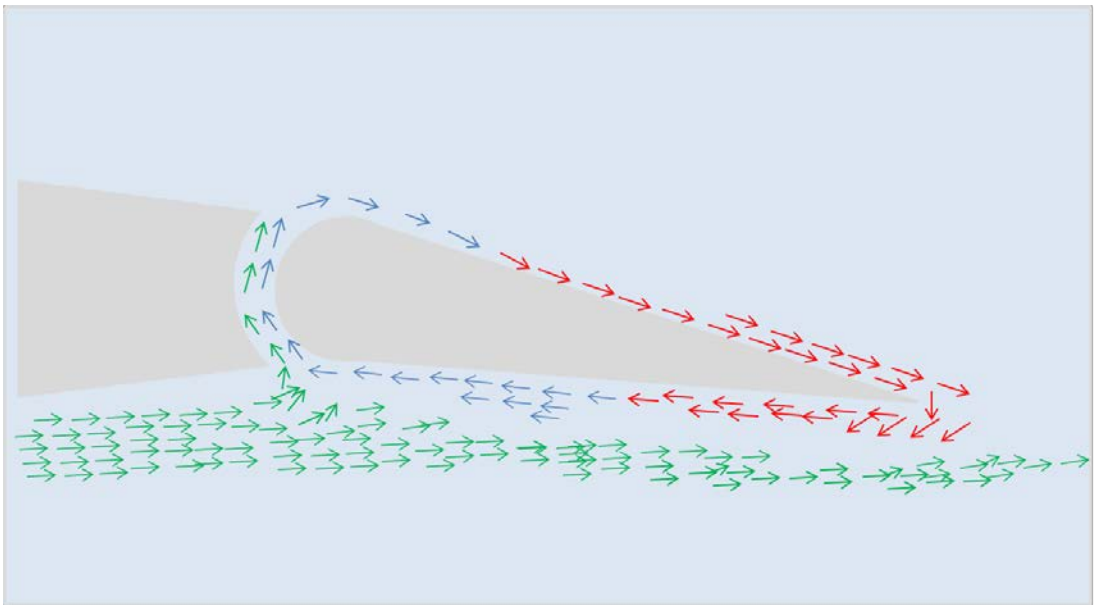

Figure 17. Schematic view of the flow pattern expected in the flap.

The full flow visualization sequence for steady cases has been documented in Figures 18 and 19. The first section shows a typical sequence of images obtained at a freestream velocity of 2 in/sec at angle of attack α=0° with gap= 2 mm and for flap angle deflections from 0° to -10° deg. The subsequent conditions mainly vary in the freestream velocity and a combination of angle of attack and deflection. On the other hand, the hinge gap was applied in 2 mm throughout the entire study.

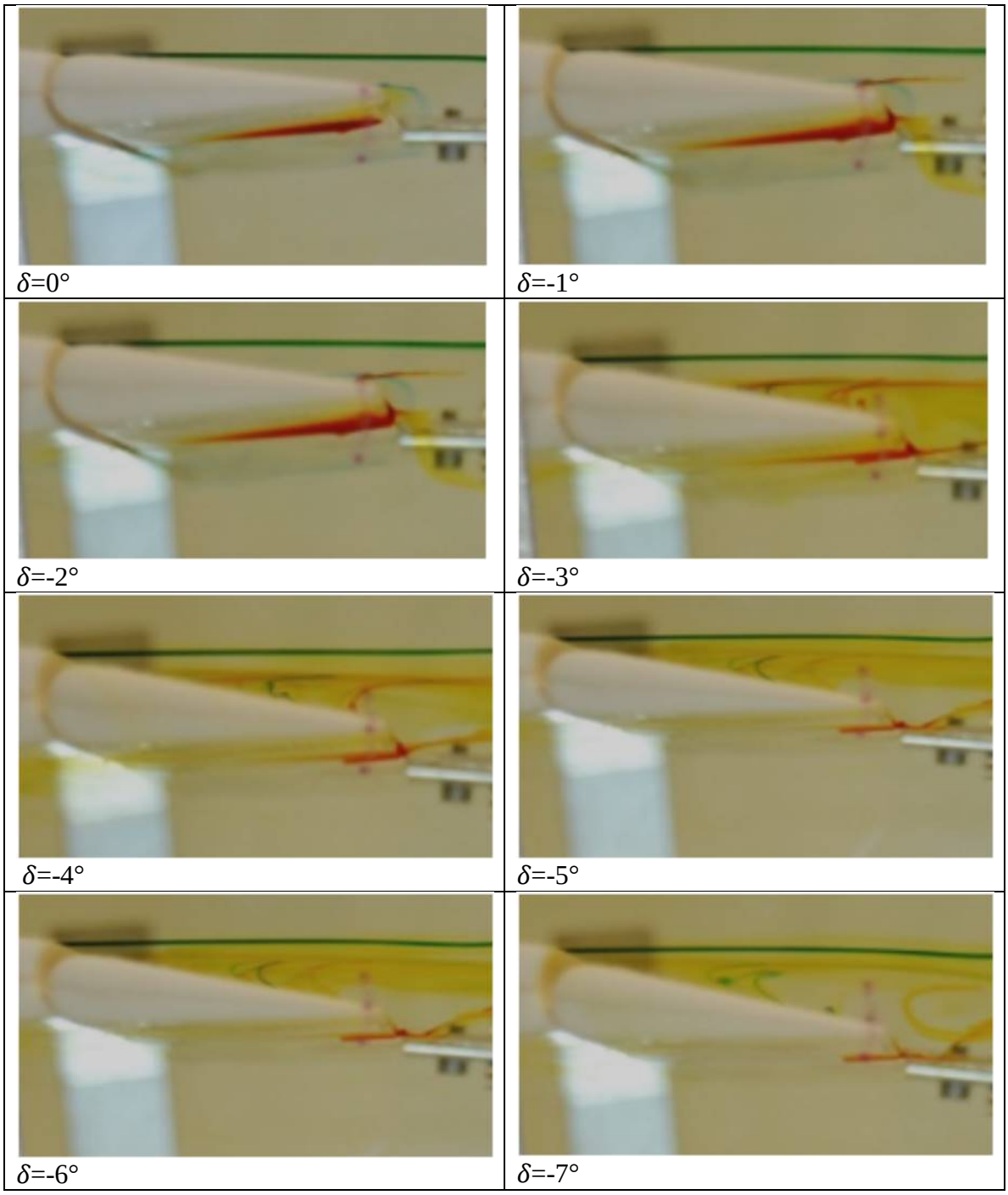

Figure 18. Steady flow pattern at U = 2 in/sec, α=0°, flap angles 0° to -7° deg.

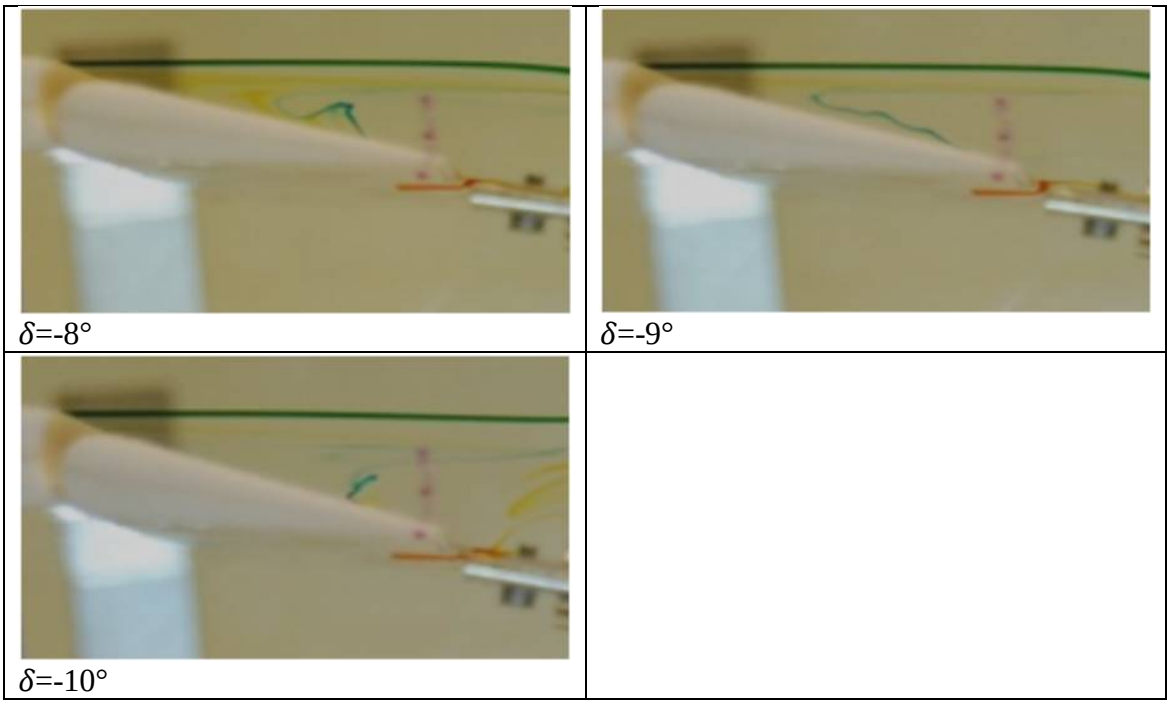

Figure 19. Steady flow pattern at U = 2 in/sec, α=0°, flap angles -8° to -10° deg.

Figures 18 and 19 present the flow at different flap deflection angles at a Reynolds number of 7,500. At this low velocity condition, the flow is laminar. The flow over the flap upper surface, which is basically the flow coming from the airfoil upper surface, presents a downstream direction when deflection is 0° deg. (case of δ = 0°). This behavior can be inferred from the blue dye performance. This feature is still present at slightly higher flap deflection angles, δ = -1° and δ = -2° deg., the flow over the flap lower surface has an increasing tendency to be attached due to the converging streamline pattern associated with accelerating flow. However, around the trailing edge, the flow has followed a direction as a manner of reversed flow in the flap upper surface. As the angle is increased further, δ = -4° deg., the whole region of reversed flow turns upstream. The upper surface flow over the flap is clearly separated. As the deflection is increased, a clockwise vortical flow seems to develop over the lower surface, which becomes fully detached at large deflection angles, δ = -10° deg.

The same airfoil variables have been used (α=0°, gap= 2 mm) for the higher speed case with a freestream velocity of 10 in/sec, see Fig. 20. At this condition, Re_c= 37,500,

the gap has a higher flow interaction than at the lower speed. The lower surface flow is moving upstream, but in a thin layer, possibly attributable to the lower surface wrapping around the trailing edge. But, the flow quickly changes and blue dye flows back through the gap as was seen earlier for the lower Re case for δ = -2° deg. For higher flap deflection angles, some rapid flow movement in the opposite direction can be seen, although it is predominantly upstream and the dye passes through the gap into the downstream side. These features were quite unexpected since the flow should have behaved as explained in Figure 16.

Focusing on the blue dye again, in Figure 20 we can see that over the upper flap surface, reverse flow is present again for δ=-1°. This flows through the gap and interacts with the reverse flow over the lower surface as can be seen from the red dye propagating upstream towards the gap. At δ=-2° this condition continues. However, once the flap upper surface flow reaches the flap lower surface, it flows downstream due to the reverse flow on the lower surface has been interrupted. At δ=-3° a transition for separation flow occurs in the upper surface, the flow in the gap as well as in the blue port dye seems to be static. At δ=-4° no flow in the gap is visualized. Once the δ=-5° the flow separation in the upper surface occurs and persists at the higher flap deflection angles. Hence, these larger deflection angles for the flap may not be able to provide the control authority necessary for effective aircraft control during landing under difficult conditions.

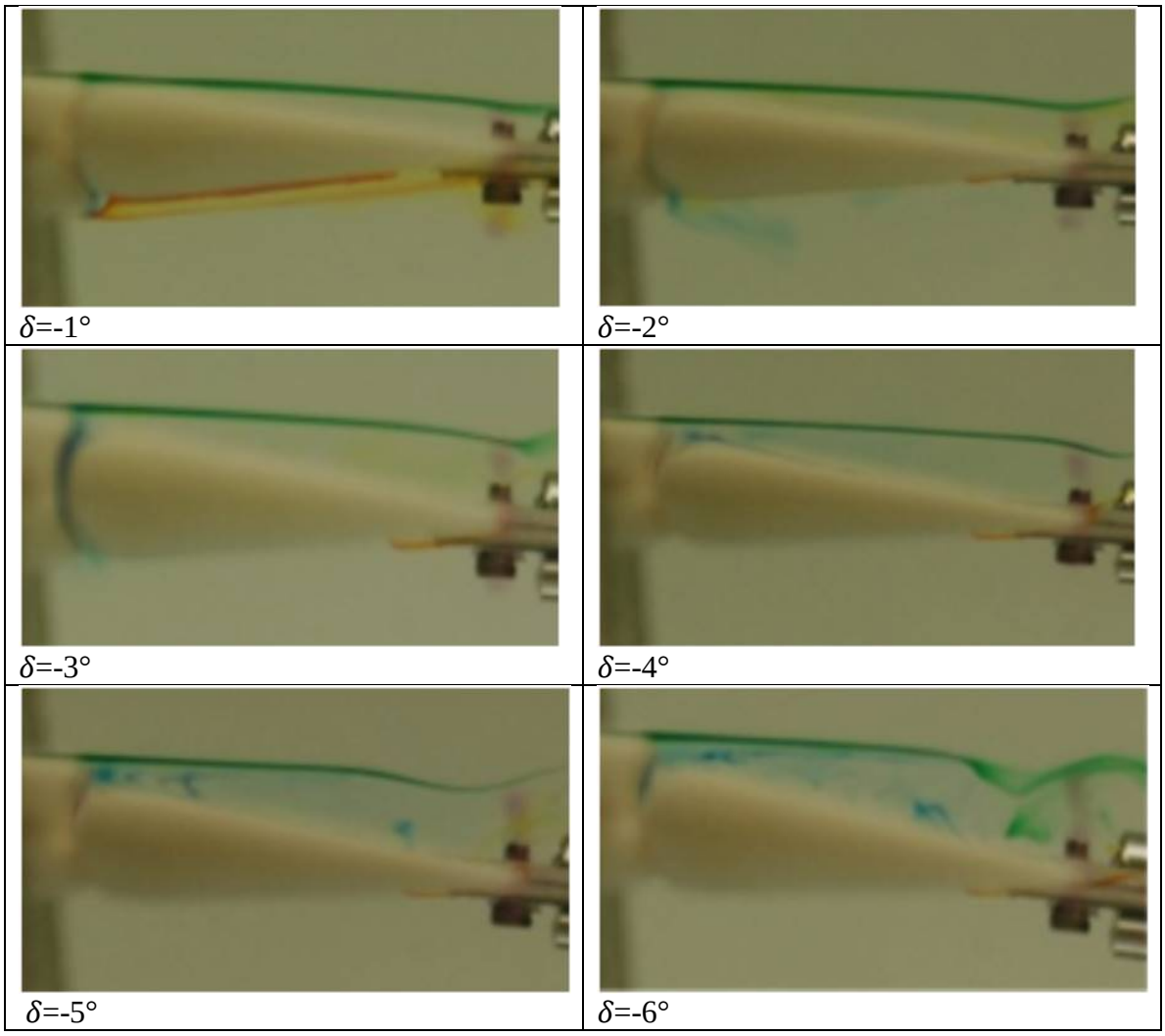

Figure 20. Movement of separation over the upper surface in steady flow pattern; U = 10 in/sec, α=0°, flap deflection angles from 0° to -6° deg.

The effect of main element angle of attack can be seen in Fig. 21 below for Re_c = 7,500. At α_{ME} = 0°, flow over the lower surface is migrating upstream, but for α_{ME} = 1° deg., it has clearly turned downstream. The blue dye seen for this case has actually arrived from the upper surface flow wrapping around the trailing edge and moving there instead of coming from the gap. For a very large deflection of δ = -9° deg., clear vortical structures are seen in the flap upper surface flow in Figure 22. These vortical structures could induce additional lift due to the low pressure in them, although the drag might also be higher.

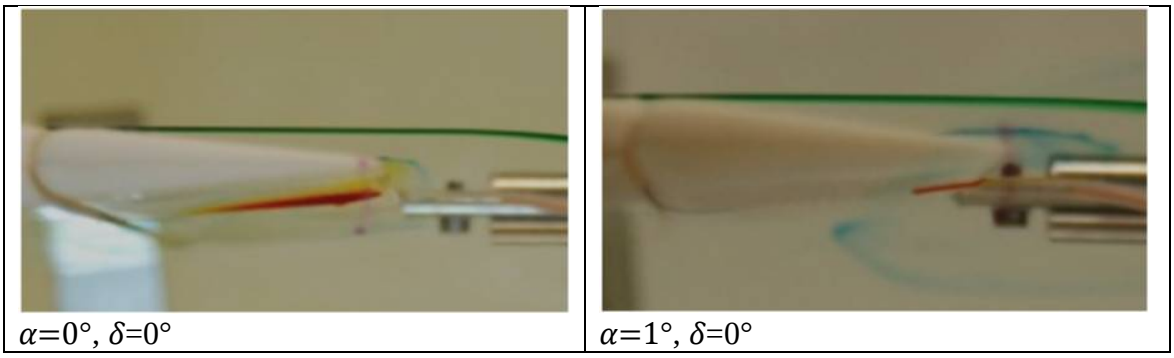

α=0°, δ=0° | α=1°, δ=0°

Figure 21. Effect of main element angle of attack at U = 2 in/sec, flap deflection angles from 0° to -9° deg.

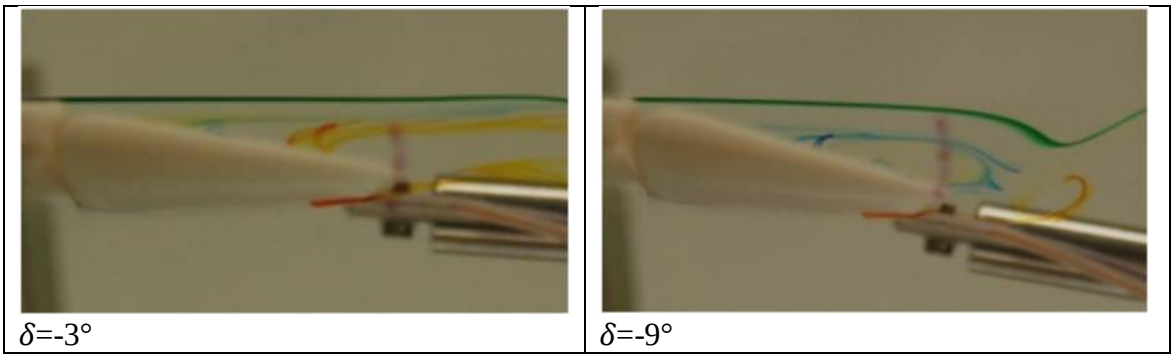

δ=-3° | δ=-9°

Figure 22. Reverse flow and recirculation in steady flow pattern at U = 2 in/sec, α=1°.

At a higher Re_c of 37,500, many of the flow features are different, for α_{ME} = 1° deg. Figure 23 shows that the lower surface flow over the flap has wrapped around and moved over the upper surface. As the flap deflection angle is increased, the upper surface flow shows a slightly increased tendency to stay attached (see green dye). However, for deflections larger than 3 degrees, the flow reverts to the separated state that it was in earlier.

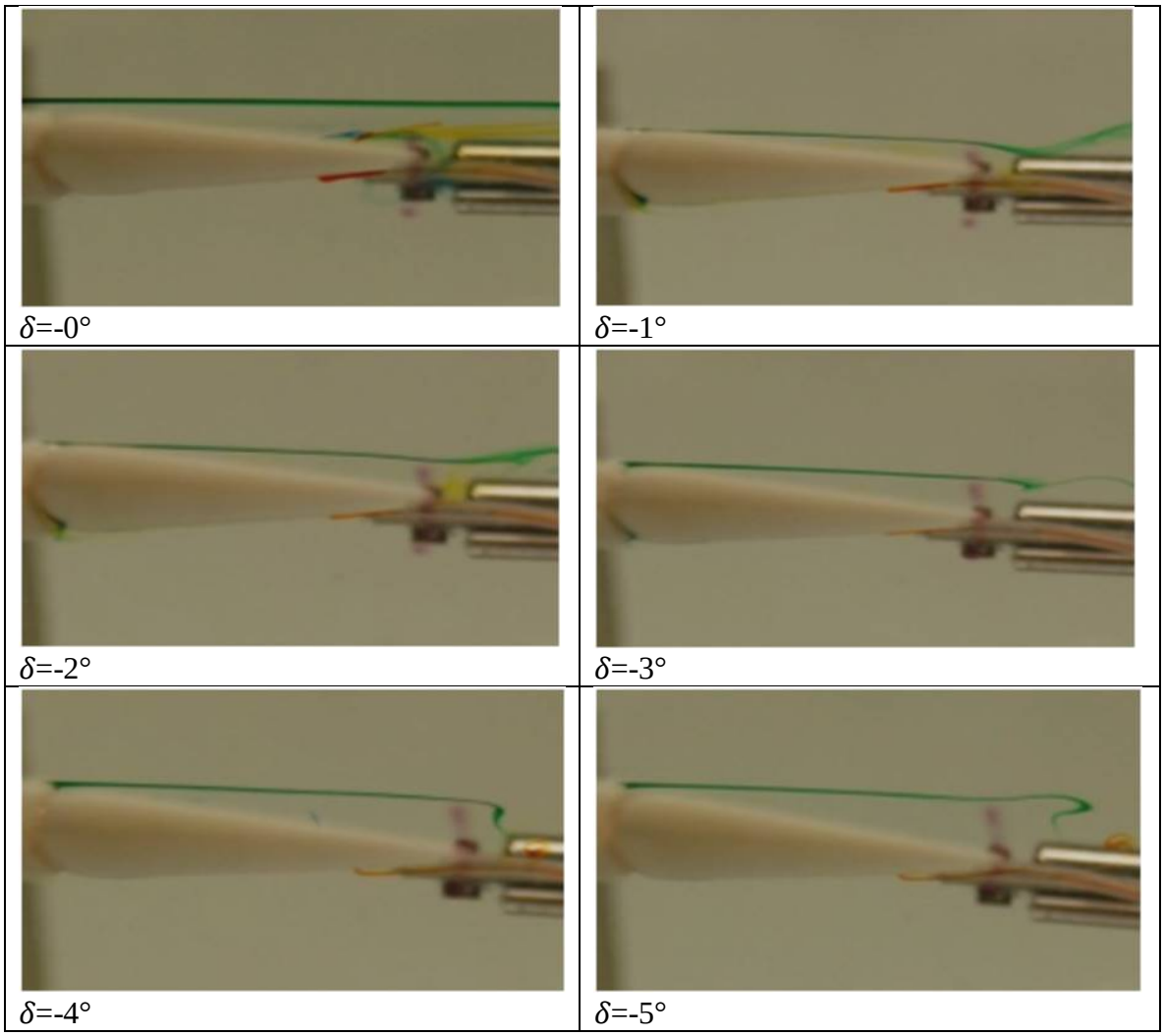

Figure 23. Reverse flow in steady flow pattern at U = 10 in/sec, α=1°, during flap angle from 0° to -10° deg.

Variations in flow pattern for an angle of attack α=2° with and flap angle deflections from 0° to -10° deg. at a freestream velocity of 10 in/sec are shown in Figure 24. At this condition, Re_c= 37,500, at δ=0° and δ=-1° the flow over the upper flap surface has reversed and even a large vortical structure is present.

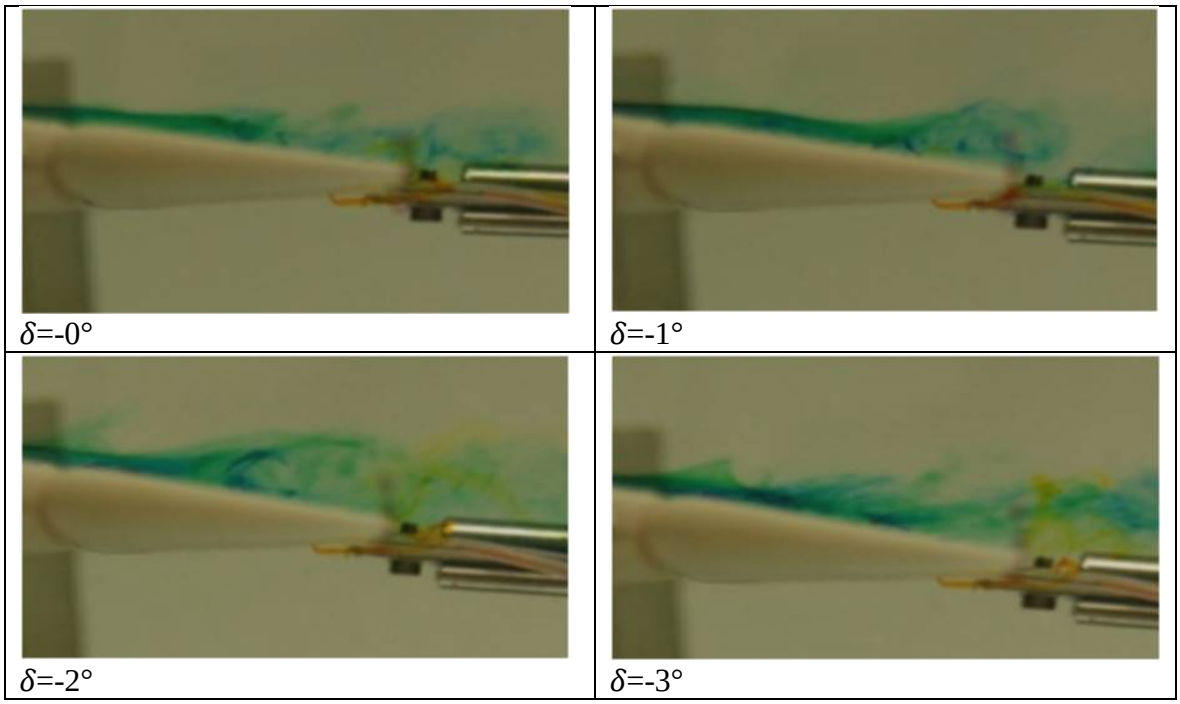

Figure 24. Separation flow in steady flow pattern at U = 10 in/sec, α=2° at flap angle from δ=0° to δ= -3 °.

It becomes evident as the flap deflection is increased (see Figure 24), it is not clear whether any useful benefits can be obtained with these settings since the flow appears to separate violently. At δ=-3^0, this vortical structure breaks down as can be deduced by the turbulent mixing seen above.

B. UNSTEADY FLOW

1. CONSTANT PITCH RATE RAMP MOTION

In this section the variations in the flow pattern produced by unsteady constant pitch rate ramp motion of the flap are highlighted. For analysis purposes, the flap ramp motion has been obtained at different amplitude (From a=1° to a=10°) in order to identify hysteresis effects and effects of unsteadiness in delaying flow separation. Due to similarities with the flow behavior in the oscillatory flap motion (explained in more detail later), just significant facts are mentioned in this section.

Figure 25 and Figure 26 show the flow visualization sequence images for unsteady flow pattern at a freestream velocity of 2 in/sec, obtained at angle of attack α=0° and flap ramp motion from 0° to -10° deg. and α^+ =0.0129. Similar to the steady condition at this low velocity condition, Re_c= 7,500 the flow is laminar. It is noteworthy here that the flow over the flap lower surface has reversed and is moving upstream (see red dye) for δ = 0°, even as the gap flow (blue dye) is running into it. At a slightly higher deflection of δ = -1° to -2°, the upstream progression of the red dye has been disrupted. However, there is still some reversed flow even at sufficiently large deflection of the flap. This is intriguing since the flow streamlines should be converging here. Moreover, much of it should be attached and moving with the freestream flow.

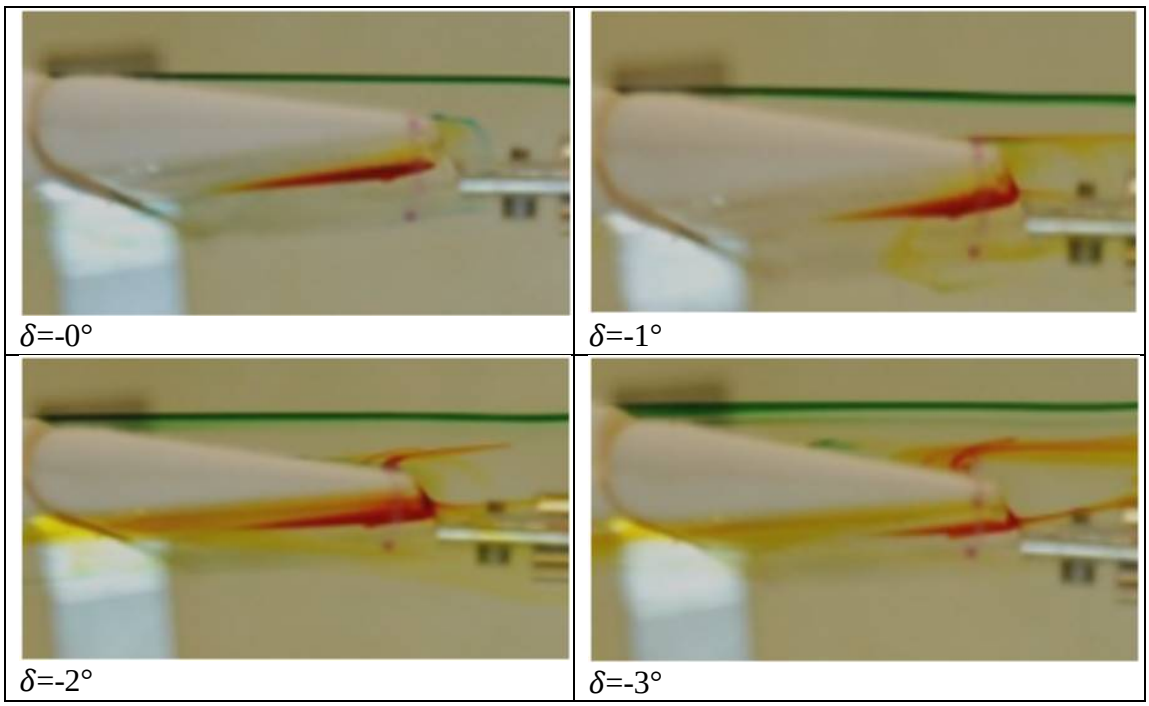

Figure 25. Unsteady flow pattern at U = 2 in/sec, α=0°, Flap Ramp Motion with different amplitudes.

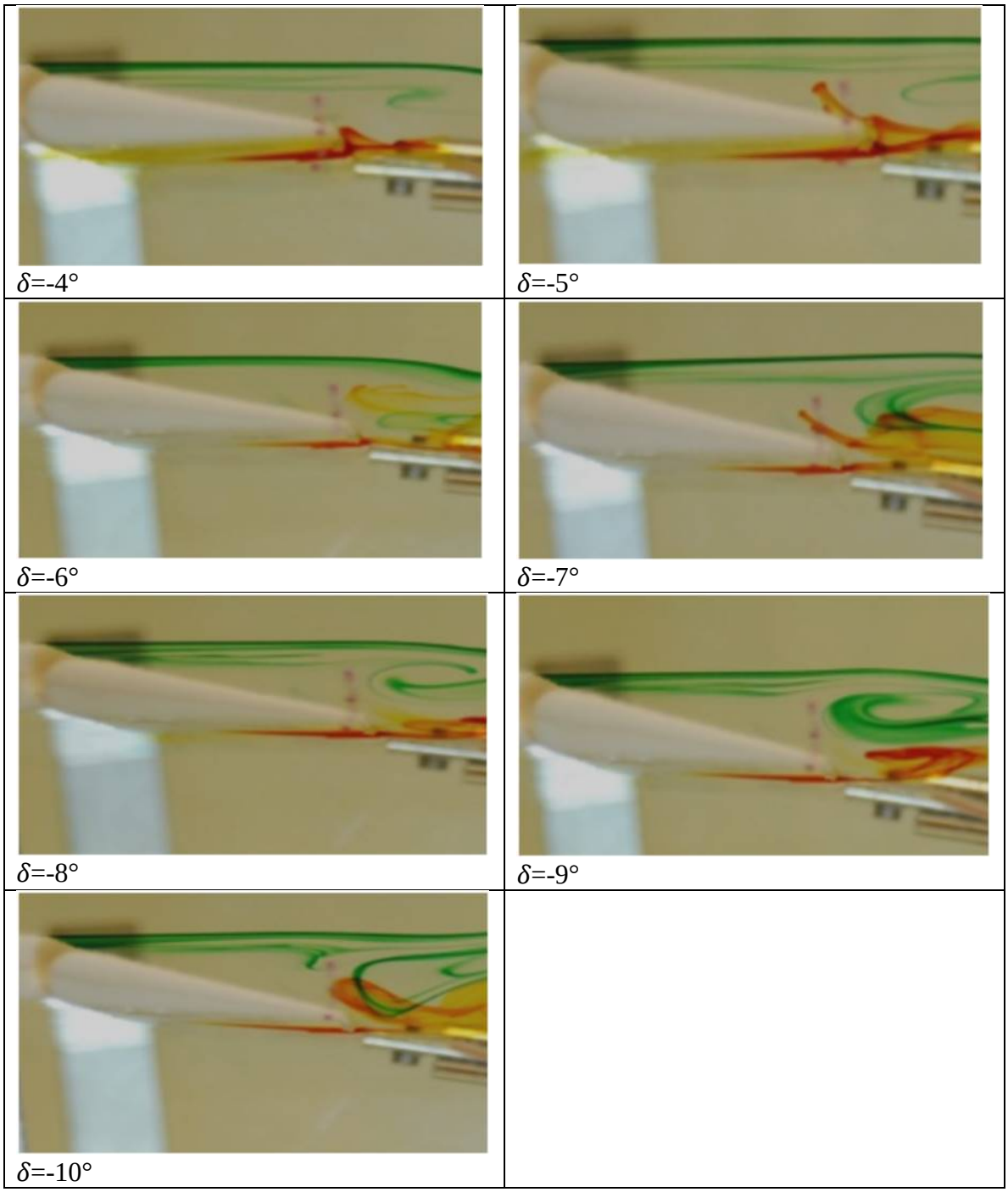

Figure 26. Unsteady flow pattern at U = 2 in/sec, α=0°, Flap Ramp Motion with different amplitudes.

Once the flap deflection is increased to an amplitude higher than δ = -4°, the wake of the airfoil is modified. As the amplitude in the flap is increased, the flow near the trailing edge reverses on to the upper surface from the lower surface. As the amplitude of pitching increases, the red-dye turns over the upper surface and starts flowing towards the trailing edge. However, another interesting feature evolves in the wake of the airfoil, and it seems to involve a flow structure that appears to be a clockwise vortex judging by the rapid turning and size of the red-dye flow pattern. This interpretation appears to agree with the results presented in the literature on dynamic stall. So, it is concluded that a mild dynamic stall vortex is present in this case. A strong interaction can be seen to be present between this vortex and the shear layer instabilities of the (green dye) separated shear layer; see case of δ=-9° in Figure 27. Also at amplitude higher than δ = -4°, no sign of reverse flow is described by the blue dye in the upper surface.

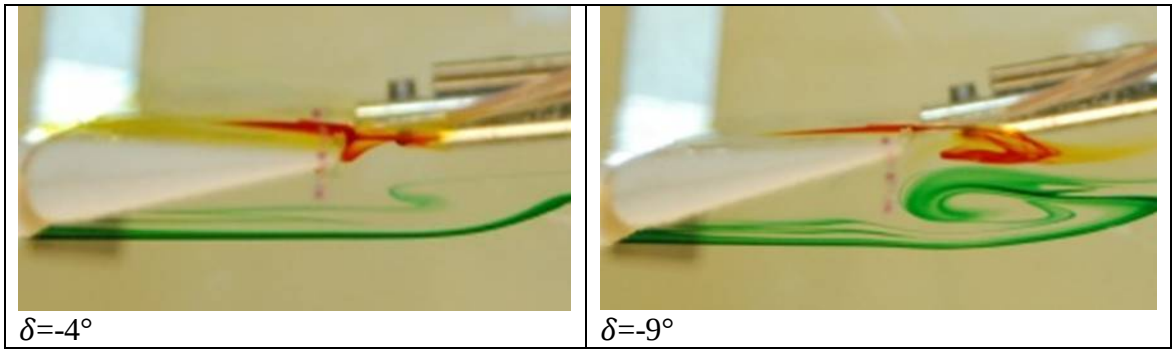

Figure 27. No sing of reverse flow in unsteady flow pattern at U = 2 in/sec, α=0°, flap ramp motion with different amplitudes.

2. HARMONIC OSCILLATORY MOTION OF FLAP

In this section the steady flow is compared with the flow produced by unsteady oscillatory motion of the flap. As described earlier, the flap was oscillated at different amplitude (from δ = -1° to δ = -10°). It is to be noted in this discussion that the maximum flap deflection equals the amplitude of oscillation.

In a manner akin to what was described for the case of ramp type pitching, a dynamic stall vortex was inferred from the flow visualization pictures presented in Figure

28 and 29. These 8 images present the flow sequence when the flow is proper and well behaved and flows downstream at zero flap deflection angle δ=0°. The red-dye starts its upstream journey by wrapping around the trailing edge and following the blue dye through δ=-6°. But, at a slightly higher angle of the flap deflection, the reverse flow is turned around and a larger dynamic stall vortex appears to form (δ=-7° & -8°). It is presumed that the differences between the ramp and harmonic cases observed is due to the differences in the non-dimensional pitch rate, which is known from the literature to have an overwhelming influence on the behavior of dynamic stall.

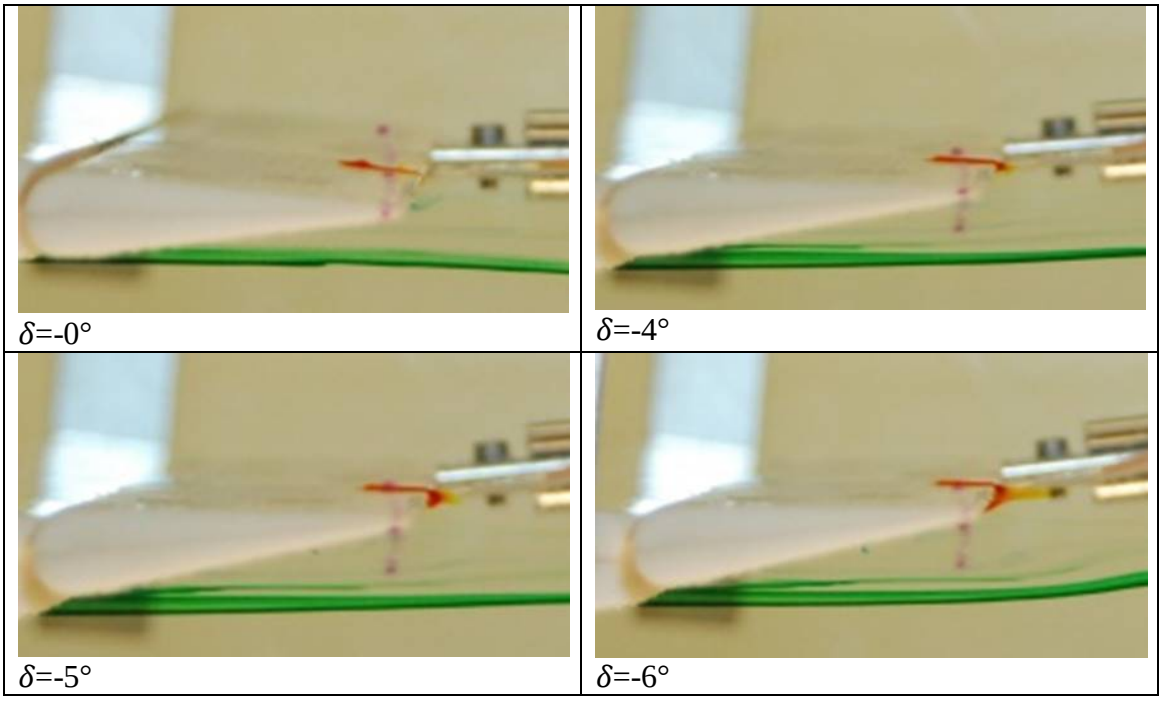

Figure 28. Unsteady flow pattern at U = 2 in/sec, α=0°, Flap Oscillatory Motion with downward flap movement.

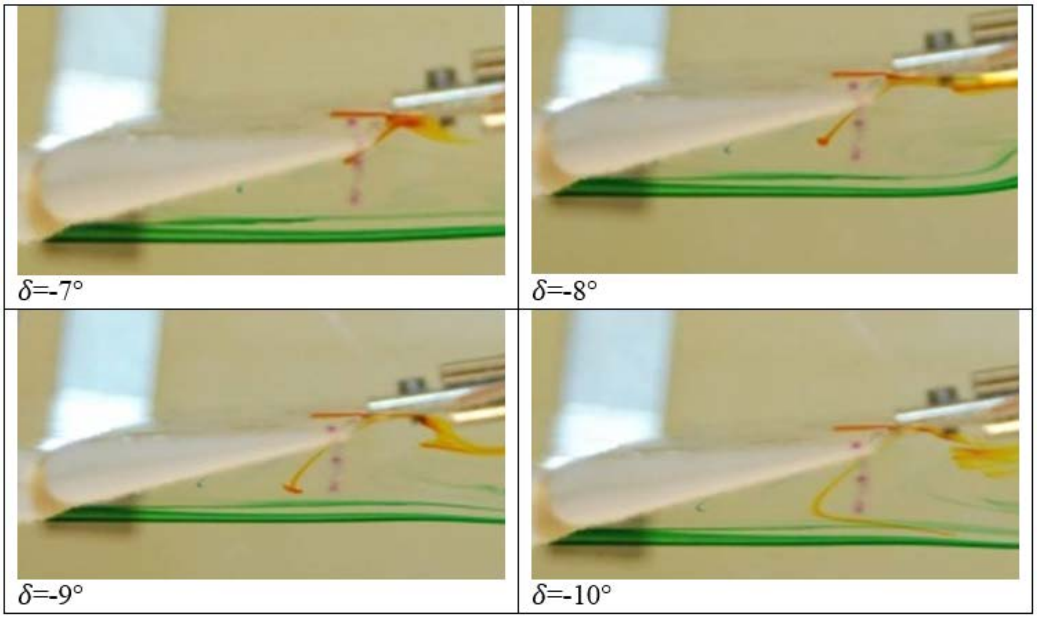

Figure 29. Unsteady flow pattern at U = 2 in/sec, α=0°, Flap Oscillatory Motion with downward flap movement.

Figure 30 shows the flow visualization images where the steady flow pattern is compared to the steady flow pattern of oscillatory flow at the same freestream velocity of 2 in/sec, obtained at angle of attack α=2° with, Re_c = 7,500. For the oscillatory condition, the flap motion had an amplitude of a= 0 to -10° deg. Similar to the steady flow condition at this low velocity condition, Re_c= 7,500, and when the flap is not deflected, the flow is laminar and the flow in the gap seems well behaved. In both cases, the flow over the upper surface of the flap demonstrates similar separated flow behavior. The flow turns around the trailing edge and seems to become vortical.

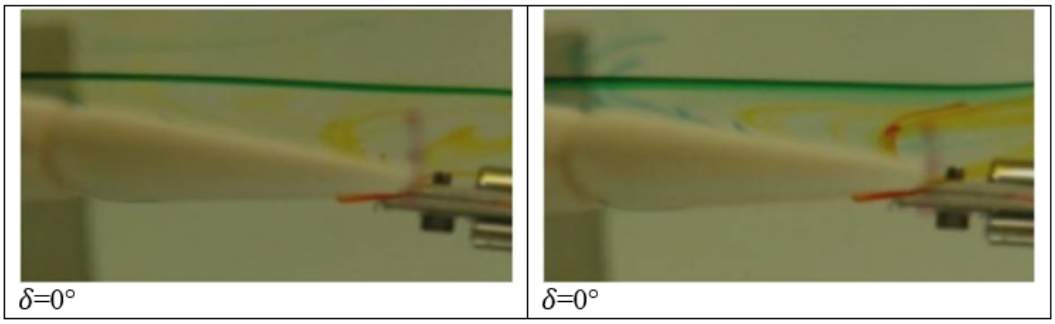

Figure 30. Comparison between steady (left) and unsteady flow pattern (right) at U = 2 in/sec, α=2° at flap amplitude δ = -10° deg.

This persists at very small amplitudes such as for δ=-1° and δ=-2°. However, for flap deflections δ=-3° a vortical behavior is visualized.

A second case is shown in Figure 31, where steady flow and unsteady flow patterns for δ=-3° are compared at the same freestream velocity and angle of attack (U= 2 in/sec and α=2°). At this stage of the movement, a vortical structure appears approximately at 80% flap upper surface. This is different from the steady flow pattern, where only a reverse flow persistently until a deflection of δ=-4°.

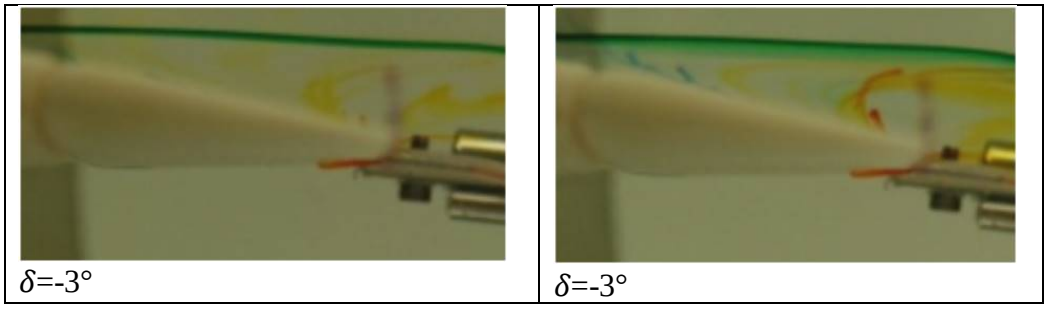

Figure 31. Comparison between steady (left) and unsteady flow pattern (right) at U = 2 in/sec, α=2° at flap amplitude δ = -10° deg.

The vortical structure over the upper flap surface lingers as the flap deflection increases further. However, once the flap deflection is at δ=-6° intriguingly, a huge bubble forms on the flap upper surface. Despite the fact that separation is present in the steady cases, it is not vorticity over the flap upper surface like in dynamic cases. Instead of that, it is reversed flow near the trailing edge that extends all the way to the gap between the two airfoil elements (Figure 32).

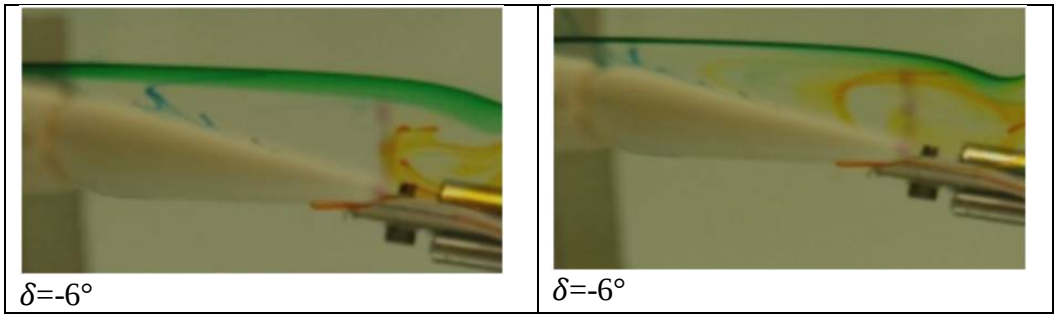

Figure 32. Comparison between steady (left) and unsteady flow pattern (right) at U = 2 in/sec, α=2° at flap amplitude δ = -10° deg.

Continuing with the flap upstroke deflection, Figure 33 presents the comparison between steady and oscillation once the flap deflection is δ=-8°. The bubble grows and spreads in both upstream and downstream directions. Additionally, the flow over the flap upper surface is completely separated.

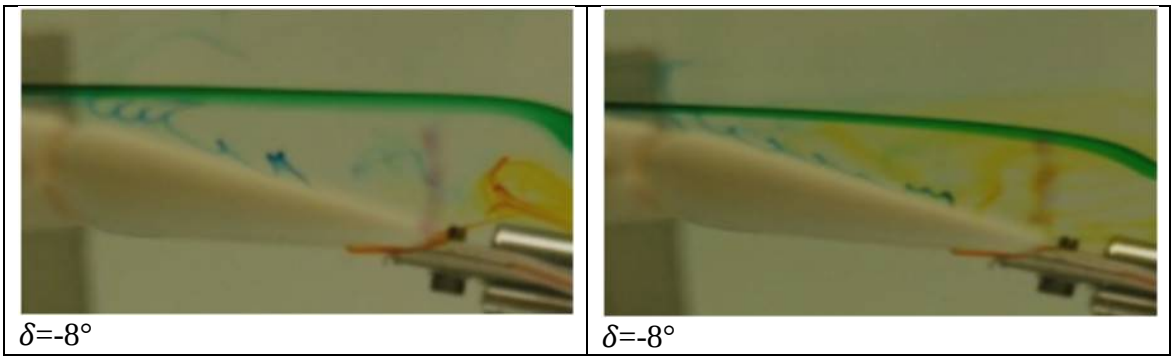

δ=-8° δ=-8°

Figure 33. Comparison between steady (left) and unsteady flow pattern (right) at U = 2 in/sec, α=2° at flap amplitude δ= -10° deg.

Once the flap has reached its maximum amplitude of δ=-10° and begins its downstroke, Figure 34 shows that the flow over the upper surface keeps moving upstream as separated flow, and eventually it turns around near the junction between the flap and main element and merges with the flow over the main element. Comparing the flow pattern in steady case at the same deflection, in both cases the separation is persistent. However, the oscillatory case is influenced by the vortical outbreak produced previously over the upper surface.

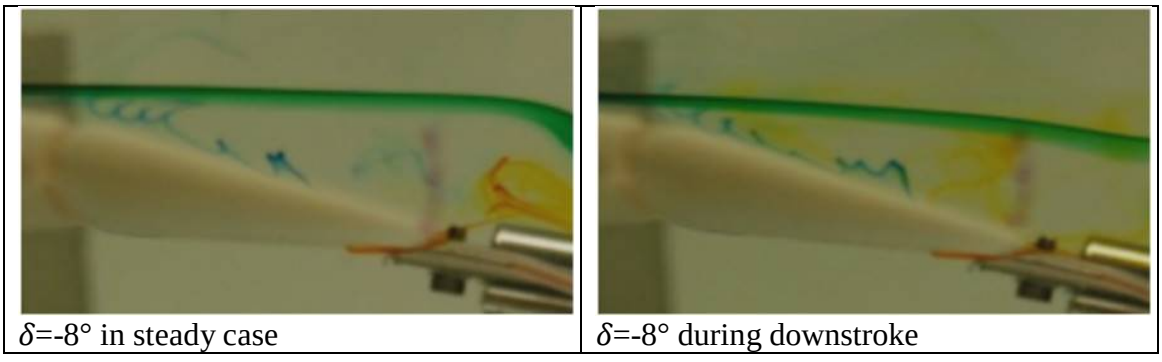

δ=-8° in steady case δ=-8° during downstroke

Figure 34. Comparison between steady (left) and unsteady flow pattern (right) at U = 2 in/sec, α=2° at flap amplitude δ = -10° deg.

What appears to be a vortex in the above discussion also suggests that a low pressure region is associated with it. Consequently, lift can be expected to be generated on the flap. The process of vortical flow formation has been analyzed with different amplitudes. As a result, it has been observed that this vortical flow pattern was not created at lower amplitudes of oscillatory motion.

In previous analysis of flow visualization cases, it has been noticed how the Re_c has a considerable effect in the presence of dynamic stall. In this case both conditions have been compared varying Re_c. In Figure 35, it is shown how at a lower Re_c (left picture) the reverse flow is present turning around the trailing edge forming a large dynamic stall vortex. Whereas that in the right picture the presence of dynamic stall is considerable attenuated at higher Re_c.

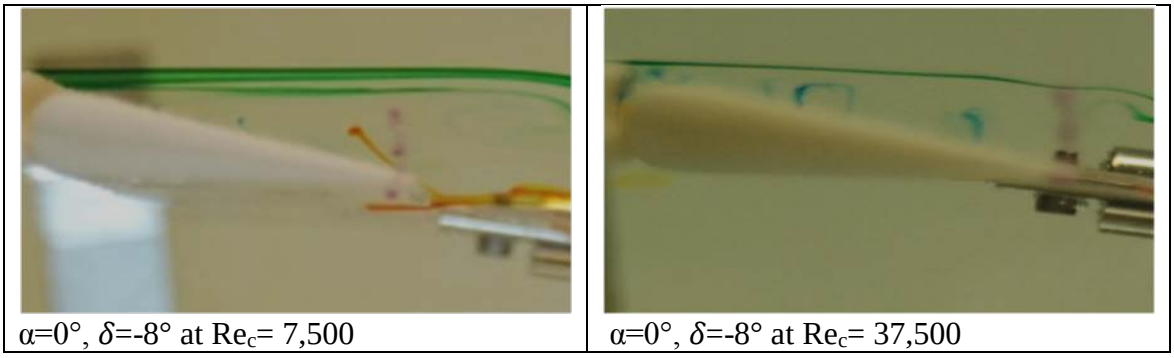

α=0°, δ=-8° at Re_c= 7,500 | α=0°, δ=-8° at Re_c= 37,500

Figure 35. Comparison of flow pattern at lower Re_c (left) with higher Re_c (right) visualized at α=0° at flap amplitude δ = -10° deg.

Finally, the oscillating flap case has been compared with the ramp flap actuation at the same freestream velocity of 2 in/sec, obtained at angle of attack α=0°. Figure 36 shows the comparison between these two unsteady cases. A clockwise vortex is clearly formed in the ramp motion (left picture) as an apparently sign of dynamic stall. Whereas in the harmonic oscillatory motion of flap (right picture) it shows how the reverse flow is near the trailing edge and it extends in gap.

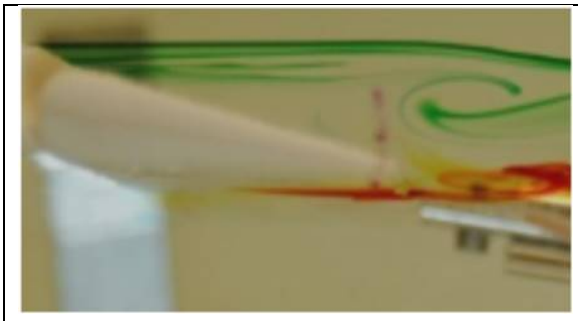

U=2 in/sec, α=0°, δ=-8° at Re_c = 7,500

U=2 in/sec, α=0°, δ=-8° at Re_c = 7,500

Figure 36. Comparison of flow pattern in flap motion (left) with oscillatory flap motion visualized at low Re_c (right), α=0° at flap amplitude δ = -10° deg.

It can be seen from these figures which basically depict low Reynolds number behavior in unsteady flows that dramatically different flow details appear when compared to higher Reynolds number flows. Low Reynolds number aerodynamics is a very challenging field of study, and these results indicate that much more detailed studies are needed. However, it is still clear that dynamic stall occurs on the airfoil even for these low Re conditions. This fact can be beneficially exploited for enhancing the maneuverability of low Re UAV.

V. CONCLUDING REMARKS

A. SUMMARY OF RESULTS

A qualitative view of the flow patterns occurring over a dynamically maneuvering trailing edge flap has been presented through a dye flow visualization study in the NPS water tunnel. Comparisons between steady and unsteady flows have been made.

In steady flow at the low Reynolds numbers of the tests, the main element upper surface boundary layer showed separation even at zero degrees angle of attack. This also resulted in a distinctly unusual flow pattern that caused the flow to move from upper surface to lower surface unlike what was expected.

In unsteady flow cases, a dynamic stall vortex was observed at very low flap (deflection) angles both for constant pitch rate motion of the flap and for the sinusoidally oscillating cases. It appears that it forms from the lower surface flow that wraps around the trailing edge and moves backwards over the upper surface. That flow is turned towards the downstream direction by the flap leading edge flow. Its evolution is rapid and appears to linger over the surface until the downstroke of the flap when it must be shed. However, this was a delayed event, occurring some time after the flap motion was reversed, well into the downstroke.

The fact that dynamic stall exists even at low Reynolds numbers is a new result. Whereas it may have been observed in flows in nature (flapping bird wings for example), the reduced frequencies that appear in such flows is significantly higher (by an order of magnitude) and so, it merits further study. These results also attest to some results of Laitone (ref. 13) who pointed out the unusual characteristics of low Re flows.

B. FUTURE WORK

In view of these intriguing results, it is suggested that even more flow visualization studies such as PIV be conducted which also provide some quantitative flow information with regard to the velocity field. Additionally, strain gage load balance

studies will help in establishing the actual lift forces under these flow conditions and allow a more thorough comparison between steady and unsteady flow cases.

LIST OF REFERENCES

[1] M. S. Chandrasekhara, M. C. Wilder, and L. W. Carr, "Competing mechanisms of compressible dynamic stall," *AIAA Journal*, vol. 36, no. 3, March 1998.

[2] L. Carr, M. Chandrasekhara, S. Ahmed, and N. Brock, "A study of dynamic stall using real time interferometry," presented at the 29th Aerospace Sciences Meeting, January 7–10, 1991, Reno, Nevada.

[3] M. S. Chandrasekhara, "A review of compressible dynamic stall control principles and methods," presented at the Proceedings of the Tenth Asian Congress of Fluid Mechanics May 17–21, 2004, Peradeniya, Sri Lanka.

[4] W. J. McCroskey, "The phenomenon of dynamic stall," NASA Technical Memorandum 81264, UNCLAS Ames Research Center_AVRADCOM, presented at von Kármán Institue Lecture Series on Unsteady Airloads and Aeroelastic Problems in Separated and Transonic Flows, Rhode-Saint-Genese, Belgium, Mar. 11, 1981.

[5] M. R. Soltani and F. R. Marzabadi, "Effect of reduced frequency on the aerodynamic behavior of an airfoil oscillating in a plunging motion," *Transaction B: Mechanical Engineering*, vol. 16, no. 1, pp. 40–52, Sharif University of Technology, February 2009.

[6] T. Lee and Y. Y. Su, "Unsteady airfoil with a harmonically deflected trailing-edge flap," *Journal of Fluids and Structures*, vol. 27, 1411–1424, 2011.

[7] S.L. Gai and R. Palfrey, "Influence of trailing-edge flow control on airfoil performance," *Journal of Aircraft*, vol. 40, no. 2, Mar.–Apr. 2003.

[8] J. S. Delnero, J. Maranon Di Leo, J. Colman, M. Garcia Sainz, F. Munoz, N. Herouard, and M. F. Camocardi, "Aspects of the influence of an oscillating mini-flap upon the near wake of an airfoil NACA 4412," FLUIDOS 2010: XI Meeting on Recent Advances in the Physics of Fluids and their Applications. Bristol, UK: IOP Publishing, *Journal of Physics*, Conference Series 296 (2011), 012007.

[9] T. Behrens and W. J. Zhyu, "Feasibility of aerodynamic flap hinge moment measurements as input for load alleviation control," presented at the Proc. European Wind Energy Association, Brussels, Mar. 15, 2011.

[10] M. S. Chandrasekhara, "Optimum gurney flap height determination for "lost-lift" recovery in compressible dynamic stall control," *Aerospace Science and Technology* vol. 14 (2010): 8, 551–556

[11] M. Meyer and Ch. Breitsamter, “Influencing the Aerodynamics of the ACFA2020 Aircraft with Flap and Trailing Edge Device Oscillations,” *Prog. In Flight Dynamics, GNC and Avionics*, vol. 6, 619–634, 2013.

[12] A.M. Rampurawala and K. J. Badcock, “Evaluation of a simplified grid treatment for oscillating trailing-edge control surfaces,” *Journal of Aircraft*, 44(4), Jul.–Aug. 2007.

[13] E. V. Laitone, “Wind tunnel tests of wings at Reynolds numbers below 70000,” *Experiments in Fluids* 23 (1997) 405–409, Springer-Verlag 1997

[14] Y. Zhou, Md. M. Alam, H. X. Yang, H. Guo, and D. H. Wood, “Fluid Forces on a Very Low Reynolds Number Airfoil and their Prediction,” *International Journal of Heat and Fluid Flow*, vol. 32, no. 1, pp. 329-339, February 2011.

[15] K. M. Issac and J. Rolwes, “Force Measurements on a Flapping and Pitching Wing at Low Reynolds Numbers,” presented at the 44th AIAA Aerospace Sciences Meeting and Exhibit 9–12, Reno, Nevada, January 10, 2006.

[16] M. Kerho and B. R. Kramer, *Research Water Tunnels*, Rolling Hills Research Corporation, El Segundo, CA, 2003.

[17] W. H. Chua, “Flow Visualization Studies Over a UCAV 1303 Model,” M.S. thesis, Department of Mechanical and Astronautical Engineering, Naval Postgraduate School, 2009

[18] M. Kerho and B. R. Kramer, *Five Component Balance System for Water Tunnel Applications*, Rolling Hills Research Corporation, El Segundo, CA, 2001.

[19] B. K. McLain, “Steady and Unsteady Aerodynamic Flow Studies Over a 1303 UCAV Configuration,” M.S. thesis, Department of Mechanical and Astronautical Engineering, Naval Postgraduate School, 2009.

[20] P. D. Sosebee, “Flow Visualization and Detailed Load Measurements Over a Maneuvering UCAV 1303,” M.S. thesis, Department of Mechanical and Astronautical Engineering, Naval Postgraduate School, 2009.

INITIAL DISTRIBUTION LIST

1. Defense Technical Information Center
   Ft. Belvoir, Virginia

2. Dudley Knox Library
   Naval Postgraduate School
   Monterey, California